International

WOCE

Newsletter

Number 21 December 1995

IN THIS ISSUE

- **News from the IPO**
  - *WOCE Data Assimilation and Synthesis* — *W. John Gould* — 2
- **Modelling and Assimilation**
  - *WOCE Synthesis and Modelling Working Group* — *Lynne Talley* — 3
  - *Mesoscale Global Ocean Circulation Modelling with Assimilation* — *Robin Tokmakian and Albert J. Semtner* — 4
  - *Variational Assimilation of Altimetric, Surface Drifter and Hydrographic Data into a Quasi-Geostrophic Model of the Azores Current* — *Rosemary Morrow and Pierre De Mey* — 7
  - *A Steady State Inverse Model of the Large Scale Circulation of the Weddell Sea* — *D.A. Nachaev, et al.* — 11
  - *A Variational Analysis of WOCE Repeat Section SR4* — *M.I. Yaremchuk, et al.* — 14
  - *NE Atlantic Circulation and Fluxes from CONVEX 1991* — *Sheldon Bacon* — 17
- **Lagrangian Measurements**
  - *Drifter Measurements in the Nordic and Barents Seas* — *P.-M. Poulain* — 19
  - *Deep Basin Experiment: Meteor Float Missions in the Southern Brazil Basin Successfully Completed* — *Walter Zenk, et al.* — 22
  - *Subsurface Float Data* — *P.L. Richardson and C.M. Wooding* — 24
- **South Atlantic**
  - *Control of the Deep Circulation in the Brazil Basin by the Sill in the Romanche Fracture Zone* — *Harry Bryden and Herlé Mercier* — 27
- **Southern Ocean**
  - *The Problem of Meridional Heat Transport in the Pacific Sector of the Antarctic* — *M.N. Koshlyakov and T.G. Sazhina* — 30
  - *Is the Deep Water Circulation in the Argentine Basin Going Round the "Wrong" Way?* — *Denise Smythe-Wright and Stephen Boswell* — 33
- **Indian Ocean**
  - *Preliminary Results From a WHP Section in the Central Indian Ocean* — *Lynne Talley and Molly Baringer* — 35
- **Tracers**
  - *Maurice Ewing Symposium on 'Application of Trace Substance Measurements to Oceanographic Problems'* — *Peter Schlosser* — 38
- **Data Issues**
  - *Second Revision of the WOCE Data Handbook* — 21
  - *Air-Sea Flux Fields Workshop* — *Peter K. Taylor* — 39
  - *WHPO Status Reports* — 26
- **Meetings Timetable** — 39

Published by WOCE International Project Office at Southampton Oceanography Centre, UK

WOCE Data Assimilation and Synthesis

W. John Gould, Director, WOCE IPO

The WOCE phase of Analysis, Interpretation, Modelling and Synthesis (AIMS) that will continue to 2002 was approved by our parent body, the Joint Scientific Committee for the World Climate Research Programme in Spring 1995. In WOCE AIMS the observations made between 1990 and 1997 and our expertise in producing global and basin-scale models will be brought together to produce, for the first time, a quasisynoptic global view of the ocean circulation that can be used to assess the oceans' impact on our climate. Bringing the models and observations together is far from a simple task. While meteorologists have considerable experience of assimilating data into their forecast models, the equivalent activity in the oceans is very much in its infancy.

The new WOCE Synthesis and Modelling Working Group chaired by Lynne Talley and Andrew Bennett met for the first time in October and started the process of planning how the AIMS phase will be carried out. It is an exciting (and daunting) challenge but considerable progress was made (see p.3-4). There will be a second meeting in Spring 1996 and possibly a third before WOCE will have a detailed, well-reasoned plan for WOCE AIMS.

Appropriately this issue of the WOCE Newsletter shows some of the results from analyses of WOCE data that go beyond simple geostrophy and that involve the assimilation of *in-situ* data into models or the reconciliation of different types of data.

Data issues

The AIMS phase really cannot go ahead until the WOCE data sets are available for researchers to use. There has been extensive discussion over the past few months on the status of data flow in WOCE. The WOCE Data Assembly Centres were specifically established to enable WOCE to maintain the high quality of WOCE data sets and to facilitate the data's transfer to and from PIs. To a large extent this has been successful and is improving. In fact, for the global One Time hydrographic survey, all data from 1992 or earlier have been submitted. There is concern that some PIs are reluctant to submit data until they have completed their own analysis. This problem has been recognised by WOCE and in an effort to encourage early submission, the following statement was adopted by the WOCE SSG in November.

> *WOCE endorses its current data sharing policy as published in "The Status, Achievements and Prospects for WOCE (1995)" (WOCE Report No 130/95). However the SSG is concerned with ensuring that all the WOCE data are submitted for preparation and documentation as quickly as possible so that information is not lost.*
>
> *Therefore the SSG accepted the current practice of Data Assembly Centres of accepting data that the Principal Investigators have not yet released for general distribution. The DACs and SACs should ensure that their procedures are such that these data are not released without the PIs authorisation. The SSG continues to endorse its policy that all WOCE data should be made publicly available within 2 years of collection.*

A further data problem is the poor submission rate for delayed-mode XBT data. While the greater part of all XBT observations are input directly (in "real time") as coded Bathy messages which enter to the Global Telecommunications System (GTS), WOCE regards this version of the data as only an interim one. Most WOCE researchers need to have access to the full-resolution "delayed mode" data after the ship returns to port. Recent experience suggests that an unacceptably small amount (as low as 20% for some years) of real-time data reappears in the delayed mode. Those who have responsibility for XBT programmes are asked to ensure that this situation improves.

The annual WOCE Data Handbook is about to be published and contains full information on the status of WOCE data sets, as do the WWW Home pages of the WOCE DACs (see p.21).

Other matters

The field programme continues apace. Soon the Indian Ocean cruises will have been completed. However it has been disappointing to hear in recent weeks that Indonesia has again refused permission for WOCE cruises to enter their waters. It was also hoped that by now we would have had a clear view of the work to be funded in the N. Atlantic in 1996-97 but the US budget delays have impacted these science decisions and it will now be February before the picture will be complete.

Next issue

Our next issue will be a new departure. Colour figures are now so much a part of the way we present our results that the WOCE Newsletter will have a 4 page colour section. The main topic will be the analysis and interpretation of XBT data. Deadline for papers on this and other topics is mid February.

The IPO send you their best wishes for Christmas and for 1996.

WOCE Synthesis and Modelling Working Group

Lynne D. Talley, Co-chairman, WOCE SMWG

The WOCE Synthesis and Modelling Working Group (SMWG) was established to provide scientific direction for the remaining years of WOCE. It replaces the committees that planned WOCE, and was specifically designed to bring observers and modellers together. The SMWG membership reflects the spread of scientific interests within WOCE. The co-chairmen, Andrew Bennett and myself, had both served on WOCE science committees devoted to modelling and observing, respectively. Our first meeting was held in Boston in October, 1995 and was attended by nearly the entire committee. The following contains preliminary conclusions from our first meeting. A complete report is forthcoming.

WOCE's principal goal is to improve ocean modelling for the sake of climate prediction. A major scientific thrust for the next few years is to assess which ocean processes are really important for climate prediction. In particular, which processes below the surface layer must be observed and modelled in order to greatly increase skill? Is there a minimum resolution in space/time for observations and models which greatly increases predictive skill?

By the end of WOCE we should have estimated heat and freshwater transports and divergences with reasonable error levels. We should be able to say something useful about the time scale and magnitude of variation. We should quantify the principal mechanisms for transporting heat, freshwater and mass - these results should be central to arguments about what mechanisms should be present in a viable ocean model. That is, what are the relative roles of the Ekman layer, subduction, convection, mixing, and the deep overturning circulation? We should greatly improve estimates of diapycnal fluxes and upwelling. Process observation and understanding should include the intermediate and deep circulation, the Antarctic Circumpolar Current, and the role of smaller scale phenomena in the general circulation.

In addition to improvements for climate prediction, the WOCE data set and modelling will result in greatly improved regional descriptions of circulation, in all ocean basins as well as in the specific Core 2 (Southern Ocean) and Core 3 (North Atlantic and Brazil Basin) regions.

Synthesis of WOCE data and improved modelling calls for equally prioritized progress in three areas: data analysis, prognostic modelling and data assimilation. The WOCE goals are written in terms of improvement of ocean modelling for climate prediction. Without adequate understanding of the ocean based on traditional data analysis, successfully reaching such a goal is not feasible. Adequate resources for ocean model development are needed to carry forward the current piecemeal progress. Ocean data assimilation, even for the goal of estimating the state of the ocean in a dynamically-consistent manner as opposed to its use in climate prediction, is still in the developmental stage.

Observations. The WOCE field observational phase is winding down in the sense that specific experiments for each ocean basin will be concluding within about two years. Left in place in each basin are programmes which are intended to continue for a long time, for instance the XBT, subsurface float, and surface drifter programmes. These essential elements of an ocean monitoring programme must be folded into CLIVAR and GOOS. WOCE data and modelling results should be used in the next few years to determine optimal sampling strategies for GOOS and to recommend field programmes for CLIVAR. The SMWG is making recommendations on data products based on WOCE observations, and considering the extent to which data analysis should be a collective effort, particularly in production of WOCE "climatologies". The SMWG will express strong support for analysis of observations based on traditional methods as well as development of techniques of data assimilation.

The SMWG urges continued support for the Data Assembly Centres (DACs), whose most important functions are to collate, quality-control and disseminate data. Easy access to the public data sets is a necessary function of the WOCE data system. Online access is recommended where reasonable.

Modelling. Ocean modelling as used in the meteorological agencies generally consists of very coarse resolution models, primarily of the upper ocean. No compelling argument has been made to the agencies that better resolution and greater attention to the deep ocean is needed. Such advances might not be possible in these agencies at present given the current computing capacity, but when computing power becomes greater, it is expected that eventually better ocean models will be used. Meanwhile it is incumbent on WOCE modelling to test the sensitivity of ocean models which might be used in future climate modelling, with respect to resolution, forcing and parameterizations. It is WOCE's role to develop the best high resolution global ocean models which will ultimately be of use in climate modelling. It is necessary for WOCE modelling to determine and demonstrate the minimum requirements for ocean modelling for climate.

Major institutional support is required for large-scale, eddy-resolving ocean models; such support has been made available in several European countries and Japan, yielding notable successes in both model development and in understanding ocean processes using the model results. In order for effective modelling on this scale to continue, adequate computer resources must be made available and at the same time, resources to support development and analysis of the model results are essential. The SMWG will evaluate the current state of modelling resources and make recommendations to the SSG and national committees. The SMWG will recommend vigorous development of

new algorithms for ocean modelling. A workshop on WOCE modelling might be recommended.

Data assimilation. This is perhaps better referred to as "state estimation", because predictive functions are not yet a reality. Data assimilation is at the stage of ocean modelling perhaps twenty years ago, with emphasis on development of techniques, reduction of error, and eventually proof of concept. It has applications at this time for ocean model testing, in which the assimilation can aid in finding large inconsistencies in models relative to observations, and to some more limited extent in hypothesis testing about ocean processes. Eventually data assimilation should provide a product which is as useful as more traditional data analysis. The advantage of the assimilated products should be dynamically consistent interpolation between observations. Reduction of model error as well as observational error is essential.

WOCE data assimilation should be supported in two modes: academic groups developing techniques and using limited data sets, and institutional group(s) developing techniques for quasi-operational assimilation, including data sets such as altimetry, XBTs, drifters and floats. The latter type of assimilation would be facilitated by an institution with a long-term commitment to the assimilation, and would include data management, modelling and assimilation aspects. Because of the nature of the data, this type of assimilation would be most relevant to the upper 1000 metres of the ocean at first, since the time series measurements with widespread spatial coverage are located there at this time and for the near future.

CLIVAR/GOOS. Many observing programmes initiated by WOCE are expected to form the basis for ongoing global measurements for climate. WOCE results should used to determine optimal sampling strategies for ongoing ocean monitoring in GOOS, and possibly also for CLIVAR field experiments. Modelling in CLIVAR is likely to be focused on coupled atmosphere-ocean models, and so it is imperative that WOCE vigorously pursues ocean model development during its remaining years. There is, as yet, no CLIVAR field implementation plan, which is a concern for WOCE. CLIVAR is holding workshops over the next year on the roles of watermass formation, large scale ocean circulation and large scale atmosphere-ocean interactions in producing climate variations on decadal to centennial time scales. There should be WOCE representation at each workshop.

The next meeting of the SMWG will be in Grenoble, France, in April. The agenda will include the SMWG's recommendations for synthesis and modelling, and a discussion of the transition to CLIVAR and GOOS.

Mesoscale Global Ocean Circulation Modelling with Assimilation

Robin Tokmakian and Albert J. Semtner, Department of Oceanography, Naval Postgraduate School, Monterey, CA 93940, USA

This is a short note to describe the improvements in the Semtner/Chervin global 1/4-degree (average) ocean circulation model and the early results from the assimilation of altimeter data into this model. The first section describes the improvements in the model formulation and the second section describes the assimilation experiment that is being conducted using this mesoscale global ocean circulation model.

Model description

The ocean model that is used for the global mesoscale assimilation is an updated version of the Semtner/Chervin model (Semtner and Chervin, 1992) which runs on a Cray YMP supercomputer. The model is a primitive-equation model with 20 levels and a Mercator grid, of a 1/4° average cell size. The model is forced by the 3-day wind stress fields interpolated from the twice daily ECMWF 10 meter wind stress fields. Climatological monthly heat fluxes (Barnier *et al.*, 1994), interpolated to 3-day fields, are used and the salt fluxes are handled by relaxing to the Levitus 1994 surface salinity values (Levitus and Boyer, 1994). The model has a prognostic free surface (Killworth *et al.*, 1991) to facilitate the nudging of the sea surface height (SSH) field towards the altimeter data and allow for realistic coastlines and bottom topography. Detailed analysis of the accuracy of the large scale circulation can be found in Stammer *et al.*, 1995. From the analysis of an eight year run (1987–1994), it was found that the model is producing realistic circulation patterns on the large scale, but is somewhat deficient in eddy kinetic energy and the uptake of heat in the top layers. This eight year model run provides the control run for the assimilation experiment described below. The assimilation experiment is initialized with the output from October of 1992 of the control run. Detailed information on the model, how to access the model output, and some animations of the model fields for various regions can be found in http://www-vislab.nps.navy.mil/~rtt.

Assimilation experiment

The assimilation of oceanographic data into a meso-scale resolution global ocean circulation model presents some difficulties that are not encountered when the assimilation of data is done regionally. The first difficulty is to find an efficient method of assimilating many types of observational data into the model. The second problem is how to effectively assimilate the observational data in all

regions of the world's oceans. And last, there is the difficulty of how best to quantify the improvement in the model's fields: U, V, W, T & S and sea surface height (SSH) when observational data is assimilated.

Large amounts of time and effort have been expended to investigate techniques for inserting altimeter data into ocean models. Ghil and Malanotte-Rizzoli (1991) provides a general review of the current state of the assimilation using ocean models. Basically, there are two types of assimilation methods, sequential and variational. Sequential methods include the very simple method of nudging to the much more complex and computationally intensive Kalman filter. Variational methods which minimize the distance between the model and data over a time interval, subject to a dynamical or smoothness constraint, are also computationally intensive. Therefore, the nudging method has been chosen for this research because of the need to limit the computation time required to assimilate data into the model.

Many different kinds of observational data can be assimilated into ocean models, for example SSH, temperatures, and salinities. However, at the present time, global temporally varying observations are limited to surface fields obtained by satellite instruments such as SST and SSH anomalies. In this experiment, the only observational data being assimilated is SSH anomalies computed from a joint TOPEX/POSEIDON and ERS-1 altimeter data set (Le Traon *et al*., 1995). The data covers the period from 6 October 1992 through 23 December 1993 (T/P cycles 6–18). ERS-1 was in a 35 day repeat and T/P is in a 10 day repeat cycle. If observational data is limited to surface data, a method must also be included to extend the surface data vertically into the layers below. Mellor and Ezer (1991) found, using a primitive equation model, that predetermined correlations between sea surface height anomalies and subsurface temperatures and salinities were required to translate surface information to the subsurface layers. This is the method that has been chosen to extend information at the surface to the layers below.

The specific equations for the assimilation follow. The height field is assimilated in a straightforward manner, namely

$$\frac{\partial \eta}{\partial t} = G + R * \left(\eta^0 - \eta^m\right), \qquad (1)$$

where m denotes model data and o denotes observational data, which in this case is the altimeter anomaly height plus a mean height of a previous model run. G is the model physics for this particular equation and R is the relaxation coefficient. R, in theory, is a function of the error in the observation field times a time difference times a space difference (Anthes, 1974). For example, R at grid point i,j:

$$R_{ij} = \varepsilon * e^{-\delta\tau / T} * e^{-\left(x^2 + y^2\right) / L_R{}^2} \qquad (2)$$

where ε is an error estimate of the model data point. In this case, ε is related to $\frac{<\delta\eta(i,j)>^2}{\max_{ij} <\delta\eta>^2}$, the normalized variance of SSH at a point. Thus, when the value is small (little variance), the point will be nudged weakly. When it is large, the model SSH will be pushed harder towards the observed value. This term attempts to include observational statistics into the model fields. The observational SSH provides the two dimensional set of predetermined ε values, calculated prior to the assimilation run. The last two terms weight the observation with respect to time and space, an exponential decay in time and a gaussian distribution in space on the order of the size of the Rossby radius of deformation (L_R). Daily, the joint ERS-1 and T/P altimeter data set is gridded to the model grid. As an observation ages over time, it is given less weight.

A similar scheme is used for temperature and salinity in the vertical:

$$\frac{\partial T}{\partial t} = G + R * F^T\left(\eta^o - \eta^m\right), \qquad (3)$$

where F_T is an additional term correlating SSH to subsurface temperature and salinity fields. A correlation function value for each model grid point can be written as:

$$F^T = \frac{<\delta T \delta\eta>}{<\delta\eta^2>}. \qquad (4)$$

Since few global temperature and salinity data sets exist that include a temporal component, the Levitus 1994

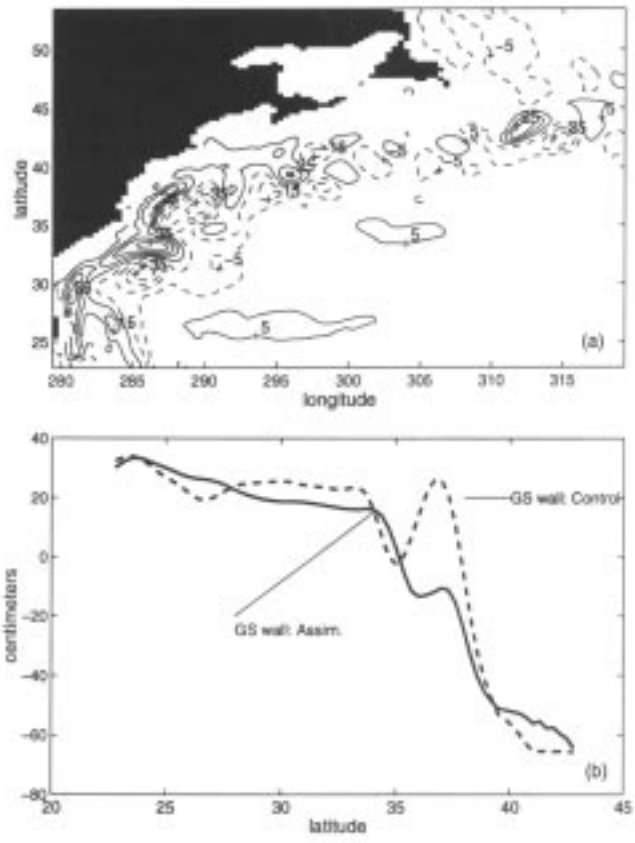

Figure 1a. Difference in the 1993 mean of assimilation run and the 1993 mean of control run in the Gulf Stream Region of the North Atlantic. Contours are every 10 cm, negative contours are dashed, positive contours are solid. 1b. Plot of mean SSH along 290°E solid line is from assimilation run, dashed line from control run.

(Levitus and Boyer, 1994) monthly climatology of T and S has been used. The covariance matrix is computed using the Levitus monthly temperature at a grid point with a monthly SSH field computed from the above altimeter data set. This produces a three dimensional set of functionals that is used in the nudging of subsurface temperature fields. A similar function, F^S, for salinity is also calculated. It might also be possible to create these global functions using data from different climatology sets for different oceans, although one would need to examine the compatibility of one data set to another. For example, the Optimum Thermal Interpolation System (OTIS) temperature data set, produced by the US Navy in the North Pacific and North Atlantic Oceans, might be used instead of the Levitus 94 monthly climatology. The method can also be modified to assimilate actual temperature or salinity values.

Initial results of assimilation experiment

Initial analysis of the data for the year 1993 shows that there are significant changes in the mean field as well as in the variability. Because of the nature of this article and the limitation of the use of black and white figures, the figures will be restricted to selected regions of the global model, hopefully giving a representation of how the assimilated data is incorporated into the model. Fig. 1a shows the difference in the mean 1993 SSH field for the Gulf Stream region of the assimilation run minus the control run. The Gulf Stream is further south when altimetric SSH data is assimilated into the model. This can be seen more readily in Fig. 1b, a plot of SSH along 290°E. Similar changes are also seen in the Kuroshio Extension region in the Pacific and in the Agulhas eddy path in the South Atlantic where SSH variability and eddy kinetic energy has increased with the assimilation of altimeter data into the model. Fig. 2 shows the difference in the RMS SSH of the assimilation run minus the control run. Notice the positive values along 35°N, corresponding to the Kuroshio Extension. Similar changes in SSH can be seen in the Antarctic Circumpolar Current as can be seen in Fig. 3. The top panel shows the instantaneous SSH field for day 365 in 1993 for the assimilation run while the bottom panel shows the same field from the control run. The middle field is the SSH field of observations to be assimilated into the model. Increases in SSH at 37°S, 25°E and 40°S, 33°E from the assimilation run match the observations seen in the middle panel. Also the width of the Agulhas current south of Africa is wider in the assimilation run than in the control run.

Heat content at a given location can be computed as in equation 5, D is equal to 360 m and T_{ref} is the mean of the temperature between 310 and 435 m (model layers 8 and 9).

$$H = \int_{-D}^{0} (T(z) - T_{ref})dz \qquad (5)$$

Fig. 4 shows the annual cycle of heat content at 35°N, 30°W in the Atlantic computed from three data sets (a) control run – solid line, (b) the assimilation run – dotted line, and (c) the Levitus 94 data set – dashed line versus

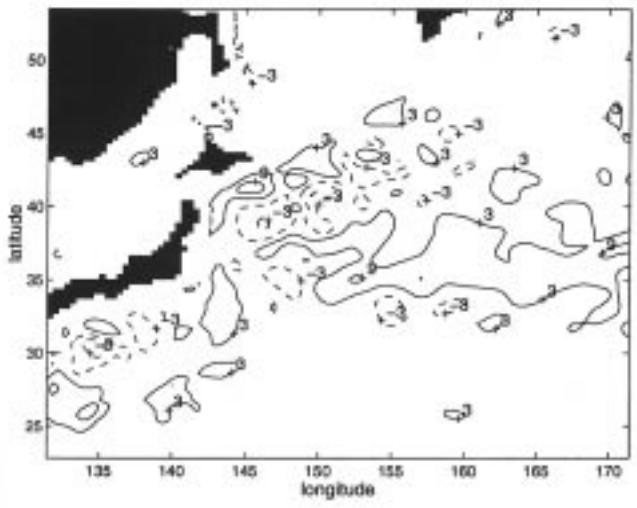

Figure 2. Difference in 1993 RMS of SSH from assimilation run and the 1993 RMS of SSH of control run in Kuroshio Extention area. Contours are every 6 cm. Negative contours: dashed; positive contours: solid.

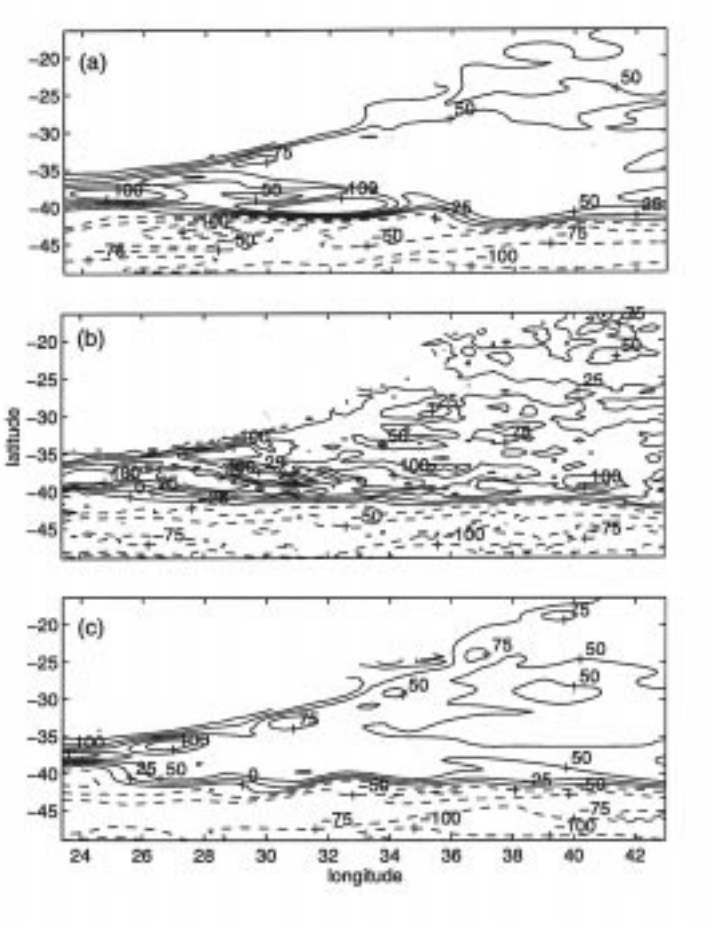

Figure 3. Contours of SSH in Agulhas Region (a) from day 365 of the assimilation run (b) Altimeter field that is being assimilated from 15 November 1993 to 15 December 1993 (c) from day 365 of the control run. Contours are every 25 cm, negative contours: dashed, positive contours: solid.

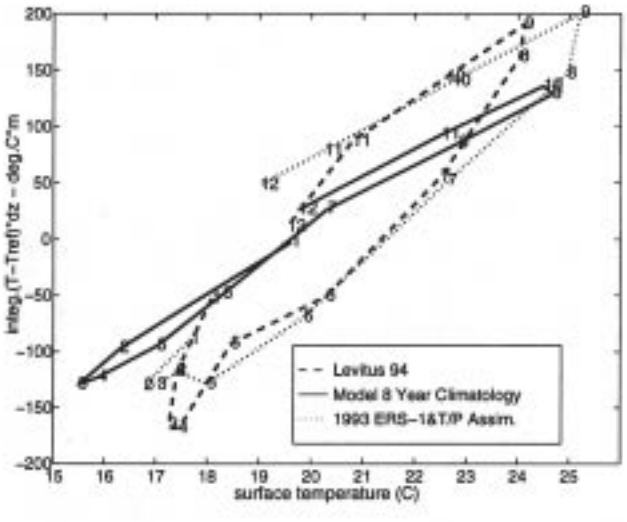

Figure 4. Monthly average of heat content in upper layers of model during the year 1993 at 35°N, 30°W. Dotted line is from assimilation run, solid line is computed from the control run and the dashed line is computed from the 1994 Levitus data set.

temperature of the model's top layer. For the control run, the heat content is directly related to the surface temperature. Contrary to this, both the heat content computed from the Levitus data and from the temperatures in the assimilation run, show a hysteresis effect. Thus, when SSH is assimilated into the model and temperature is adjusted using a cross correlation factor relating to SSH and temperature, the model's heat content is more representative of the seasonal changes.

Future plans

The initial evaluation of the assimilation of altimeter SSH data into a global mesoscale ocean model gives encouraging results that the model is adjusting to the addition of observational SSH data. The assimilation of altimeter data will continue with TOPEX/POSEIDON data and with ERS-1 when it is again in a 35 day repeat through the end of 1995. With a three year data set (1993–1995), global analysis should produce reliable statistics to judge the effectiveness of this assimilation method. Prior to continuing the assimilation, some investigations will be conducted into how the method can be improved, for example, should another T/S monthly climatology be used in a specific region or should there be changes in the relaxation coefficients to increase the effectiveness of the assimilation.

Acknowledgement

This work is funded by the National Science Foundation's Physical Oceanography Program under WOCE and the Department of Energy's Office of Health and Environmental Research under CHAMMP (Computer Hardware, Advanced Mathematics, Model Physics). We thank AVISO for making the joint ERS-1 and T/P data set available. Computing resources are provided mainly by the National Center for Atmospheric Research.

References

Anthes, R.A., 1974: Data assimilation and initialization of hurricane prediction models. J. Atmos. Sci, 31, 701-719.

Barnier, B., L. Siefridt and P. Marchesiello, 1994: Thermal forcing for a global ocean circulation model from a three year climatology of ECMWF analyses. J. Mar. Sci., in press.

Ghil, Michael, and Paola Malanotte-Rizzoli, 1991: Data assimilation in meteorology and oceanography, Advances in Geophysics, 33, 141-266.

Killworth, P.E., D.J. Webb, D. Staniforth, and S.M. Patterson, 1991: The development of a free-surface Bryan-Cox-Semtner ocean model. J. Phys. Oceanogr., 1333-1348.

Le Traon, P.Y., P. Gaspar, F. Ogor, and J. Dorandeu, 1995: Satellites work in tandem to improve accuracy of data. EOS, 76 (39) , 385 & 389

Levitus, S. and T.P. Boyer, 1994: World Ocean Atlas 1994, Volume 4: Temperature, NOAA Atlas NESDIS 4. U.S. Dept. of Commerce, Washington, D.C.

Mellor, George L., and Tal Ezer, 1991: A Gulf Stream model and an altimetry assimilation scheme. J. Geophys. Res., 96, 8779-8795.

Semtner, A.J., and R.M. Chervin, 1992: Ocean general circulation from a global eddy-resolving model. J. Geophys. Res., 97, 5493-5550.

Stammer, D., R. Tokmakian, A.J. Semtner, and C. Wunsch, 1995: How well does a 1/4 degree global ocean model simulate large-scale observations? Submitted to J. Geophys. Res.

Variational Assimilation of Altimetric, Surface Drifter and Hydrographic Data in a Quasi-Geostrophic Model of the Azores Current

Rosemary Morrow and Pierre De Mey, UMR39, Groupe de Recherche de Geodésie Spatiale, 18 av. Edouard Belin, 31055 Toulouse, France

Azores Current

The mesoscale dynamics of the Azores Current region are investigated by assimilating various oceanographic data sets into a multi-level quasi-geostrophic (QG) open ocean model. The study site lies in the path of the Azores Current in the northeast Atlantic, in a region of quite complex dynamics. The Azores Current enters the model domain from the west as a predominantly zonal jet, where it interacts with a series of sea-mounts before branching to the east and south (Fig. 1). Bottom topography is an important part of the regional dynamics, and so has been

included in our QG model. The variability generated downstream of the sea-mounts is large for an eastern boundary and is well documented in current meter data and surface altimetric analyses. The seasonal component is significant, with the possible influence of Rossby waves propagating from the east in winter. The change in regime from summer to winter is fairly sudden, but can provide a good test for the mesoscale forecasts produced by different assimilation techniques. An additional complexity is the presence of meddies, which may not be represented well by the QG dynamics.

Data

Our model domain was chosen as it encompasses the site of the recent SEMAPHORE experiment; an intensive field programme in 1993/94 which included *in-situ* hydrographic measurements during cruises, and the deployment of surface and RAFOS drifters and long-term current meter arrays. The *in-situ* data will firstly provide an independent test for the assimilation of surface altimeter data in our regional model, in particular to test the model response at depth. The data can also be assimilated directly to make use of their complementary information, *e.g.* lagrangian drifter data includes a consistent mean and eddy signal, the subsurface hydrographic data can correct the model baroclinic structure at depth.

Model and assimilation

The model we use is the multi-level Harvard open ocean QG model of Miller *et al.* (1983), but we apply two different assimilation methods. The initial conditions for our model runs are derived from the continuous assimilation of altimetric data using optimal interpolation (OI) methods (Dombrowsky and De Mey, 1992). OI assimilation is purely statistical and yields robust convergence over long periods of time, but its short-term forecast capabilities can sometimes be deceiving. The first part of the project is to see whether assimilation via the adjoint variational scheme of Moore (1991) can be applied to optimise this initial guess field, and improve the mesoscale response over 20–30 day periods. The benefit of the adjoint assimilation is that it explicitly makes use of the actual model dynamics; the individual data measurements force the model dynamics directly, without needing a separate analysis of the data distribution or its statistical properties. Longer term forecast fields from the two methods will be compared at the end of summer, when the dynamical regime changes abruptly.

We apply the adjoint variational method to improve the OI analyses, in our limited area O(1000 km^2) multi-level model; during periods when irregularly-spaced, dense datasets are available such as cruises or drifter deployments. Thus the second aim of the project is to assimilate a variety of different oceanic data sets, and evaluate their importance in constraining the QG model. In this way, the adjoint assimilation can provide a quantitative test of data compatibility with the chosen model dynamics. A number of practical concerns for the adjoint assimilation are given in detail in Morrow and De Mey (1995).

Assimilating satellite altimetric data

Satellite altimetry from TOPEX/POSEIDON (T/P) and ERS-1 altimeters were assimilated into our QG model over a 20-day period in July 1993. Only the variable component of the altimetric signal can be resolved accurately, so for the assimilation we also subtract a climatological mean field from the model. The alongtrack altimeter-plus-mean height measurement is assimilated directly at its closest model grid point, both in space and time. For display here we have created 10-day maps of the combined T/P and ERS-1 data in Fig. 2a using optimal interpolation. 10-day maps provide complete T/P data coverage, which has a groundtrack spacing of around 285 km at this latitude, *i.e.* too large to really resolve the mesoscale dynamics. The ERS-1 data has a better eddy-resolving groundtrack spacing of around 130 kms at this latitude, although its 35-day repeat cycle means only around 1/3 of the region is sampled in 10 days. The Azores Front is clearly shown meandering around 34°N, and bifurcating to the east and south around 22.5°W. Surface drifters (circles) released in the second half of the period clearly converge at the Azores front, and in good agreement with the frontal position derived from altimetry. The main features show only minor evolution over the 20-day period, consistent with the regional time scales measured from other data sets of O(30 days).

The model is run forward from its initial conditions with no further assimilation, as shown in Fig. 2b. In fact this is not a pure simulation run for two reasons. First, although our initial conditions are derived from a 7-day OI forecast field, the OI analysis step uses weighted data from 30 days each side of the analysis time. So data from this

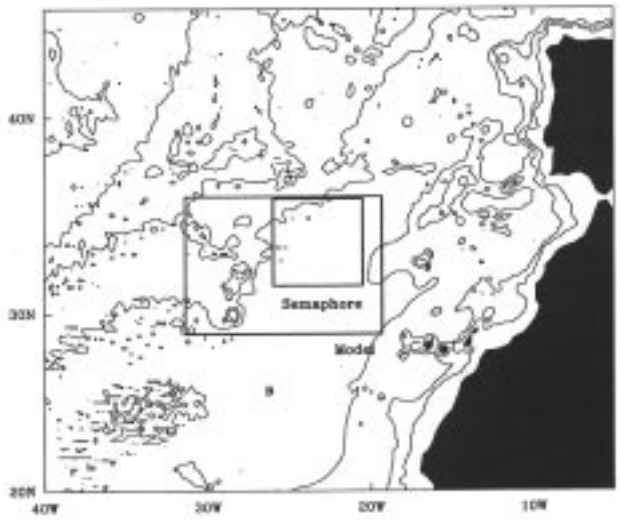

Figure 1. The model domain in the Azores Current region, showing the bottom relief (CI=1000 m), and the SEMAPHORE region.

entire 20-day period has been used in the previous OI analysis on 22 June 1993. Secondly, our model boundary conditions are interpolated at every model time-step from 7-day OI forecast fields, so also include future data. Using the 7-day forecasts from the OI assimilation provided reliable and stable initial guess fields (Fig. 2b). This occurs at all model levels, and the bottom flow remained strongly constrained by the model topography. In comparison to altimeter data, the model run starting from OI has a stronger and more zonal jet, with fewer meanders. In general, the positions of the eddies each side of the front are fairly well modelled after 20 days.

The adjoint assimilation of the combined surface altimeter data was very effective in optimising the initial conditions, so that the surface fields remained closer to the data during the 20-day model run (Fig. 2c). The position and amplitude of the model eddies are now closer to the observed, as is the position of the meandering front, especially in the SEMAPHORE domain. The adjoint assimilation reduces the misfit between the model and the data during these 20 days by 50–80%, depending on the chosen data constraints.

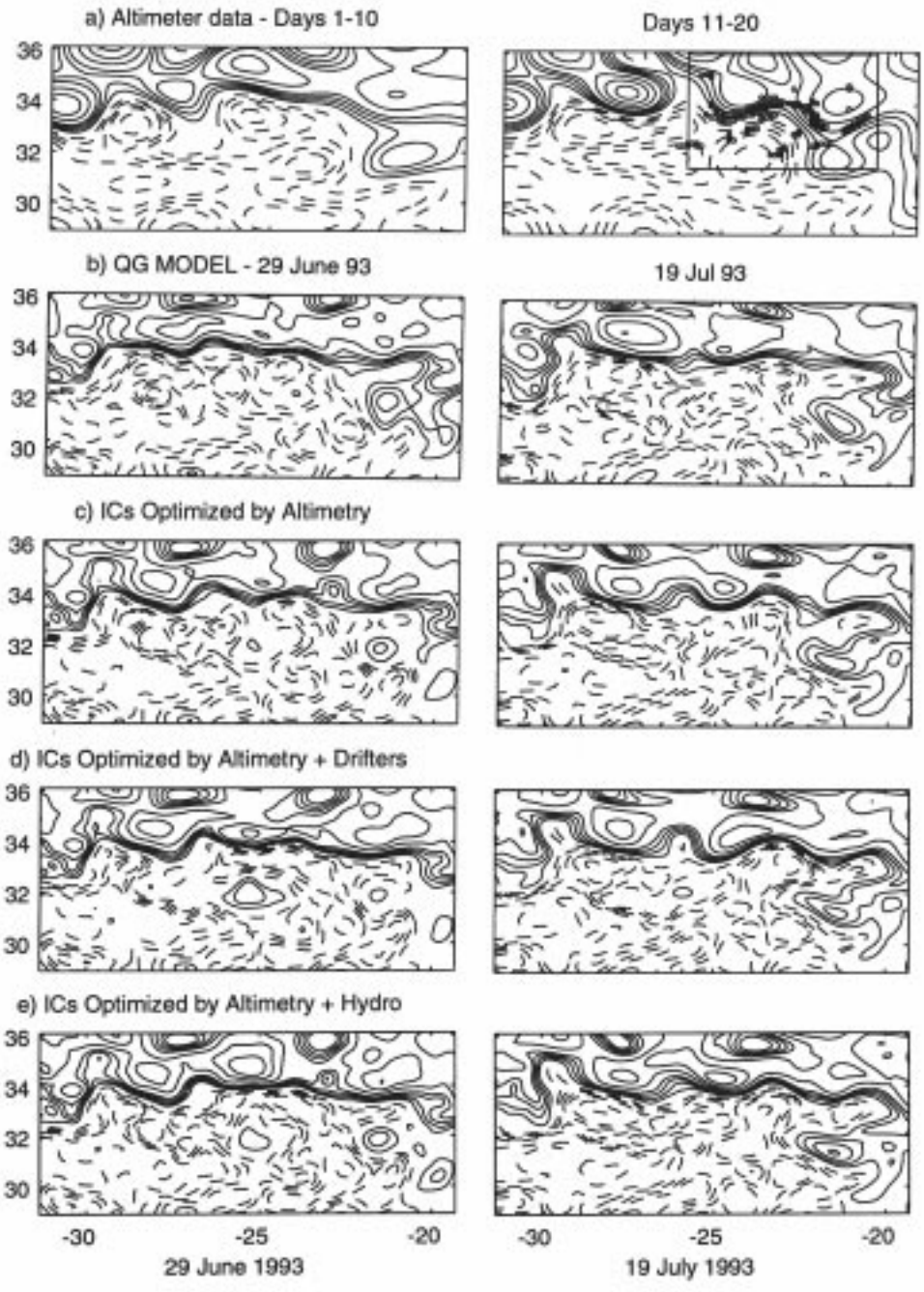

Figure 2. Surface streamfunction in the model domain in non-dimensional units. (a) 10-day altimeter data maps, with surface drifters (o), and the SEMAPHORE domain for the hydrographic data (-). The model initial and final conditions are also shown for a 20-day model run starting from (b) 7-day OI forecast fields at 29 June 1993, with no further assimilation; (c) initial conditions optimised by T/P and ERS-1 altimetry, (d) ICs optimised by altimetry and surface drifters, (e) ICs optimised by altimetry and hydrography.

Altimetry proved to be a good constraint on the variable flow field, and appeared particularly strong in adjusting the barotropic field. We tested the T/P and ERS-1 assimilations separately, as well as the combined data set shown here. The improved data quality of the TOPEX/POSEIDON altimeter data provided smooth and reliable forcing. But for our mesoscale studies, the extra spatial coverage from the combined T/P and ERS-1 data sets was important for constraining the solution and providing stable flow at all levels. Because the adjoint model acts like a 3-D filter on data noise, the differences in the altimeter data sets due to different noise, corrections or mean fields was minor in comparison to the benefits from the improved data coverage.

Assimilating surface drifter data

Surface drifters were an excellent constraint on the variable field – again constraining both the barotropic and baroclinic fields in the assimilation. More importantly, the drifters provide a reliable measure of the mean field. The mean and the variability are assimilated as a consistent measure, which is not the case with the altimetric assimilation where the mean is derived from an independent (and smooth)

climatology. The result is that surface drifter assimilation provided a much stronger mean jet during our assimilation period (see the SEMAPHORE domain in Fig. 2d), which extended down to 2000 m depth.

Assimilating hydrographic data

Assimilating hydrographic data (Fig. 2e) brought similar changes to those from the drifter assimilation. The vertical structure of the model was weakly improved by constraining the vertical pressure modes. However, the strengthening of the mean jet was consistent with the drifter measurements; and there was a transfer of energy from the barotropic to the first baroclinic mode at the position of a meddy (at 36°N, 24°W). The difficulty with the hydrographic assimilation was to separate its effects from the stronger altimetric assimilation. In our model a second data constraint was always necessary; the hydrographic constraint alone was unstable as it could not constrain the faster barotropic mode. Although the vertical adjustment from the hydrographic assimilation was minor within our 20-day assimilation period, it played an important role in stabilising the longer-term forecast runs.

Forecast runs

Does this improvement remain valid for longer time periods in 'pure' forecast mode. To test this, we have run the model forward over a 2-month forecast period, starting from both the unoptimized 7-day forecast fields from OI and the optimized initial conditions from the 20-day adjoint assimilation of different data sets. The boundary conditions for the 60-day run are again taken from OI forecast fields during this period. Note that data from the first 20 days has been included via assimilation in all of the initial conditions (adjoint and OI).

Figure 3a–c shows the misfit between the model variables and the altimeter, drifter and hydrographic data sets during the 2-month forecast, for each different set of initial conditions. For all model runs the surface stream-function shows a gradual divergence away from the measured altimetric field. The run starting from OI initial conditions has the largest misfit. The run with initial conditions optimised by altimetry remain closer to the altimetric data by 50% throughout the 2 month period, and are also closer to the independent drifter data (Fig. 3b). Assimilating altimetry by either the OI or adjoint method makes little difference in regard to the misfit with hydrographic data (Fig. 3c). However, the adjoint assimilation of drifter data also reduces the independent hydrographic misfit, and *vice versa*. Both *in-situ* data sets significantly improve the baroclinic structure in the model, which is important in the forecast runs since the model variability is principally driven by baroclinic instabilities.

Including drifters in the optimisation degrades our results in comparison to the altimeter data, which probably indicates that the altimeter mean is wrong. Hydrography and altimetry tend to provide a more consistent measure.

Are our optimised model runs better than simple persistence? Fig. 3d shows the ratio of the rms forecast error to the persistence error for each run. The run with initial fields from OI is much better than persistence over the first 10 days (*i.e.* 17 days from the analysis time); thereafter it remains only as good as persistence. However, all the adjoint optimised forecast fields are 20–30% better than persistence throughout the 2-month period. In particular, the fields optimised by *in-situ* data are still at the 0.8 level at the end of the forecast period. Thus the adjoint assimilation not only reduces the cost function within the 20-day assimilation period, but also can improve the longer-term forecasts of mesoscale dynamics over a period of 2 months.

Acknowledgements

We wish to thank Andy Moore for the adjoint code, P-Y. Le Traon (TOPEX/POSEIDON data), Eric Dombrowsky (ERS-1 data) and Fabrice Hernandez (surface drifters). The hydrographic data collected during the SEMAPHORE

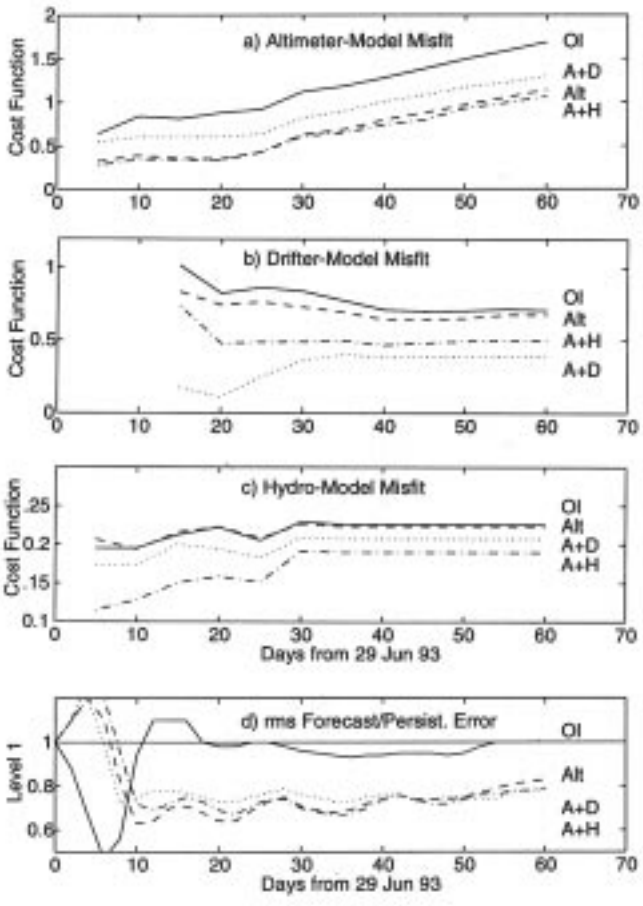

Figure 3. Data-model misfits for the 2-month forecast run starting from different optimised initial conditions, for (a) altimetry, (b) surface drifters and (c) hydrography, (d) rms forecast/persistence score for each model run. The initial conditions are from OI (OI,-), or with ICs optimised by altimetry (Alt,- -), altimetry + drifters (A+D,...), or altimetry + hydrography (A+H, -.-).

campaign was provided by SHOM. The assimilation study was supported by DRET, France.

References

Dombrowsky, E., and P. De Mey, 1992: Continuous assimilation in an open domain of the Northeast Atlantic. Part I: Methodology and application to AthenA-88. J. Geophys. Res., 97(C6), 9719–9731.

Miller, R.N., A.R. Robinson and D.B. Haidvogel, 1983: A baroclinic quasi-geostrophic model open ocean model. J. Comput. Phys., 50, 38–70.

Moore, A.M., 1991: Data assimilation in a quasi-geostrophic open-ocean model of the Gulf Stream region using the adjoint method. J. Phys. Oceanogr., 21, 398–427.

Morrow, R.A., and P. De Mey, 1995: Variational assimilation of altimetric, surface drifter and hydrographic data in a quasi-geostrophic model of the Azores Current. J. Geophys. Res., (in press).

A Steady State Inverse Model of the Large Scale Circulation of the Weddell Sea

D.A. Nechaev, M.I. Yaremchuk, and J. Schröter, Alfred-Wegener-Institute for Polar and Marine Research, 27515 Bremerhaven, Germany

Hydrographic data from the Weddell Sea are assimilated into a steady state circulation model. We diagnose a solution which is in geostrophic balance and conserves mass and buoyancy. The model is driven by surface fluxes and inflow/outflow at the open boundaries. The boundary conditions and the forcing fields are adjusted in order to get the steady state solution which is closest to the hydrographic data. The inverse model has been called a p-model because the surface pressure is used as a control variable. For a given surface pressure field we can calculate the full three dimensional current field using the momentum equation. The internal pressure which is needed for this calculation is taken from the density field which in turn is determined by advection. The procedure is iterative and allows the estimation of a consistent solution, *i.e.* the currents are consistent with the density structure and the density field is a solution of the advective-diffusive equation for buoyancy conservation applied to the models velocity field.

Assimilation scheme

Climatological data for the Weddell Gyre taken from the Southern Ocean Atlas (Olbers *et al*., 1992), the annual mean ECMWF wind stress and transport estimates (Yaremchuk *et al*., 1995) derived from data collected from 1989 to 1993 on WOCE repeat section SR4 are assimilated into a numerical model describing the steady state circulation at low Rossby numbers. A variational data assimilation technique is used where the model state is optimized in the sense of a prior probability distribution which is specified by a cost function. The steady state model is weakly constrained by three 2D fields in the measurements of sea surface elevation ζ, wind stress $\vec{\tau}$ and surface buoyancy flux B.

The numerical model employs a set of well-known dynamical constraints commonly used in literature for description of the steady state large scale circulation. These include linearized steady state momentum equation (geostrophy plus 3D diffusion), hydrostatics, continuity and the steady state buoyancy advection-diffusion equation. The buoyancy constraint is satisfied 'weakly' since the dynamical system allows small deviations from the advective-diffusive balance, which are penalized by the cost function. The same 'weak' formulation is used for the boundary conditions involving sea surface elevation, cross-surface fluxes of momentum and buoyancy and the bottom velocity field. The cost function contains four major groups of terms:

1. Terms penalizing model-data misfits. Data on ζ and B were obtained from various indirect sources and have extremely low weight in the cost function. Model transports across the WOCE section SR4 were also weakly attracted to the values obtained after assimilating these data into a separate inverse section model (see Yaremchuk *et al.*, 1995).
2. Regularization terms, enforcing horizontal smoothness in the control fields and in the streamfunction.
3. Terms, penalizing errors in the buoyancy equation and in the bottom boundary condition.
4. Exponential penalty for states with hydrostatically unstable density profiles.

Inversions of the covariance matrices, which describe prior estimates of statistical scatter of the different cost function entries around their respective mean values, were derived either empirically or from the data sets, if available. All the matrices were taken as diagonal, some depending upon spatial coordinates. For instance, we assumed larger sub-grid variability in the coastal regions for the fields of buoyancy, surface elevation and total transport, reducing the corresponding weights. By variation a distinct minimum of the cost function could be achieved. The function itself is reduced to 2% of its initial value which was computed using the standard dynamical method for the diagnosis of the velocity field.

The resultant optimal state exhibits only a small

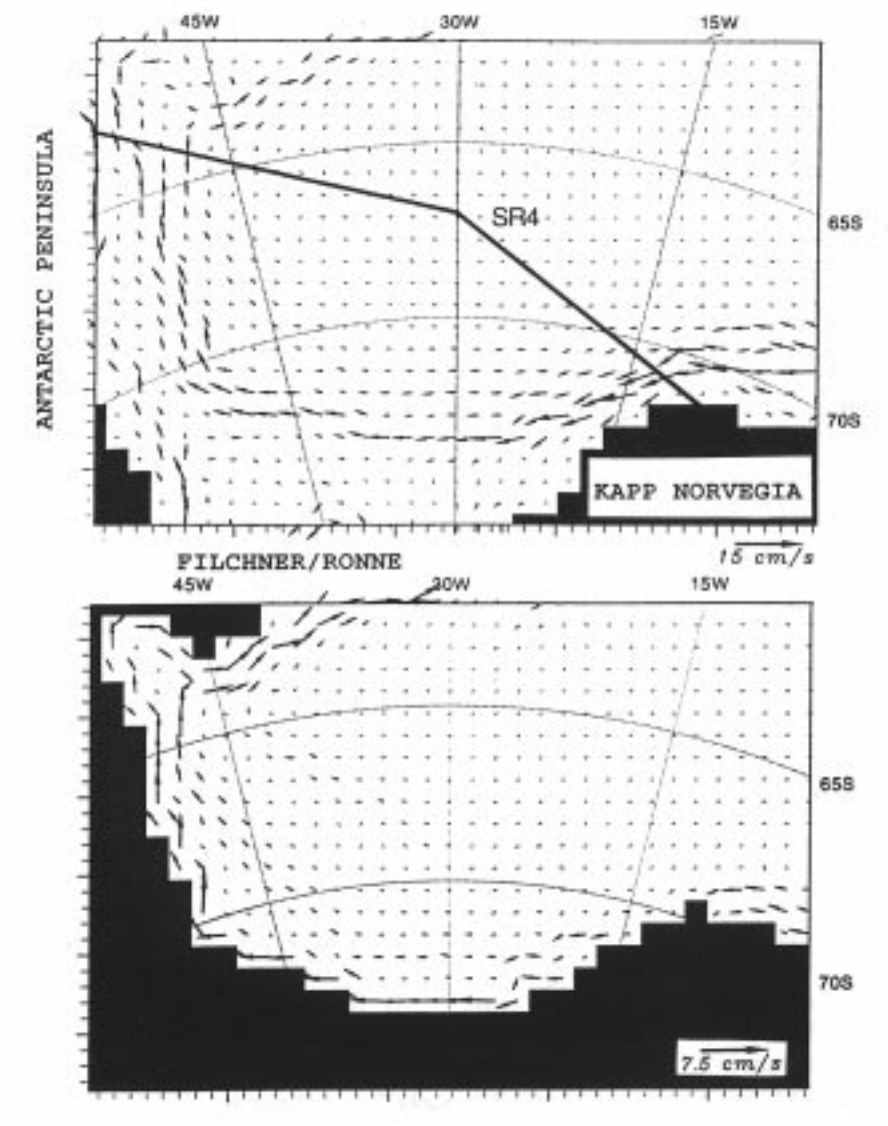

Figure 1. Steady state velocity fields at the levels of 30 (top panel) and 2740 m depth (bottom panel).

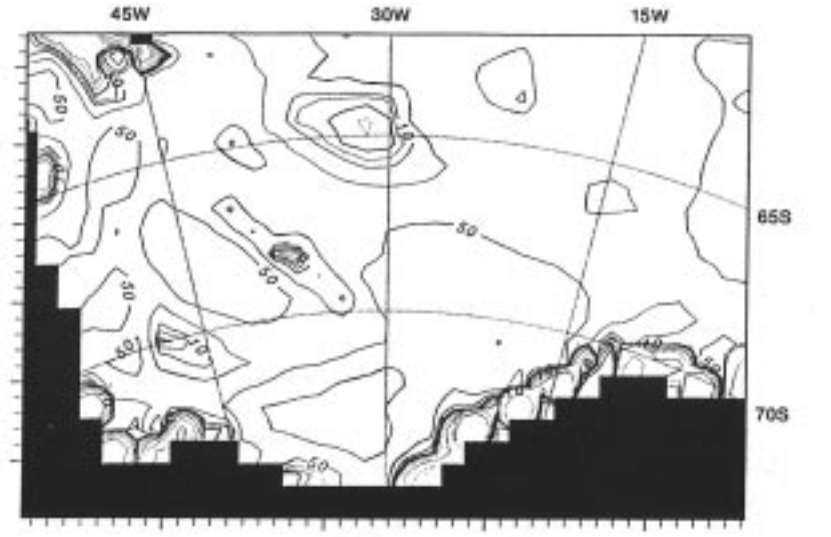

Figure 2. Horizontal distribution of the steady state vertical velocity field in metres per year at a depth of 570 m. Bold contours separate regions of upwelling and downwelling.

temporal trend in the buoyancy field. Model-data misfits in the fields of buoyancy and wind forcing were found to be consistent with the error bars of the underlying data.

The model domain covers the Weddell Gyre (Fig. 1). In the north and the east, open boundaries connect the model to the deep ocean. Instead of including the shelf along the Antarctic Peninsula in the model domain we preferred to use open boundaries there. By this we may indirectly estimate water mass modification on the shelf by processes which are difficult to model directly. The open boundary at the south is connected to the continental shelf at the Filchner/Ronne Ice-Shelf. The density field along the boundaries and simultaneously the consistent flow field are determined from the interior data alone. This means for instance that for the southern boundary we can give a rough estimate of the circulation south of the model: inflow and outflow as well as modifications of water masses on the shelf are calculated by the inverse model.

The transect SR4 connecting Kapp Norvegia with the tip of the Antarctic Peninsula crosses the model domain almost diagonally.

Steady state circulation

Transports and mass balances. The finite difference scheme of the model conserves mass within the accuracy of the net transport into the bottom boundary layer (residual error in the bottom boundary condition). The latter was found to be 0.004 Sv and directed out of the boundary. It agrees with the concept of the bottom Ekman pumping induced by the clockwise circulation of the Weddell Gyre. Another constituent of the mass transport balance is a considerable net inflow of 0.019 Sv coming from the southern open boundary neighbouring the Filchner/Ronne Ice-Shelf. A part of this inflow leaves the model domain within the western boundary current flowing along the shelf of Antarctic Peninsula.

Fig. 1 shows horizontal velocity patterns at 30 and 2740 m depth. The major feature seen on the map for 30 m is a gradual decrease of the current speed as the flow proceeds along the shelf break of the Antarctic continent. On the other hand we observe a gradual increase at 2740 m

depth. This fact corresponds to the concept of downwelling at continental slopes partly attributed to Ekman transports and partly to a more intense cooling in these regions. The net transport of the Gyre is 32 Sv, in good agreement with the data. Horizontal distribution of the vertical velocity shown in Fig. 2 exhibits a number of physically sensible features: an average upwelling of 30 to 50 m yr^{-1} in the open sea and intense downwelling at the continental margins of Antarctica ranging within 1-2 km yr^{-1}. The corresponding downward water transport from the upper 300 m layer amounts to 4.5 Sv, if the integration is performed between 300 and 4000 m isobaths. The local downwelling in the centre of the Weddell Sea is most probably an unrealistic feature.

Cooling processes may possibly characterize the circulation south of the model domain on the shelf area at the Filchner/Ronne Ice-Shelf (Fig. 3). An intense inflow confined to surface layers is transformed into a deep reaching outflow in the western part of the section. The total circulation on the shelf is estimated as 1.8 Sv.

Buoyancy fluxes. The outflow from the Filchner/Ronne Shelf is estimated from the steady state balance in the interior of the Weddell Sea alone. We find a considerable transport of negative buoyancy at a rate of $512 \cdot 10^3\ \mathrm{kg\,s^{-1}}$. The diffusive flux of the same quantity is found to be almost 16 times smaller and amounts to $62 \cdot 10^3\ \mathrm{kg\,s^{-1}}$. If we assume that the annual mean salt budget is zero (precipitation + melting = evaporation + freezing, see Fahrbach *et al.*, 1994), then sea water modification on the Filchner/Ronne shelf south of 75°S can be attributed to the thermal flux through the surface $S_R = 3 \cdot 10^{11}\,\mathrm{m^2}$, of this domain giving us an estimate of the annual mean cooling rate q on the shelf of $q = 90\,\mathrm{W\,m^{-2}}$.

The corresponding indirect estimate for the steady state circulation pattern on the shelf along the Antarctic Peninsula indicates an outflow of negative buoyancy at a rate of $110 \cdot 10^3\ \mathrm{kg\,s^{-1}}$ for advection and $0.4 \cdot 10^3\ \mathrm{kg\,s^{-1}}$ for diffusion.

By analysing the transports of various water masses across the SR4 section we may calculate rates of water mass formation for the area between this transect and Antarctica. In the present study we utilize an approximation to spatial water mass classification, following Fahrbach *et al.*, 1994. Transports through the corresponding subdomains at the WOCE SR4 section indicate that the Warm Deep Water (WDW) inflow of 4.5 Sv is transformed into 2.1 Sv of Weddell Sea Bottom Water (WSBW), 1.4 Sv of Weddell Sea Deep water (WSDW) and 1.0 Sv of Surface Water (SW), demonstrating good agreement with the results of Fahrbach *et al.*, 1994, who obtained the following transformation scheme: 6.0(WDW) $\rightarrow$ 2.6(WSBW) + 1.2(WSDW) + 2.2(SW).

Diffusive terms in the buoyancy budget together with its error field of E_ρ account for the model analogues of water mass transformation processes occurring in nature. We assume that E_ρ might have a significant bias towards these processes which are poorly described by the model. Thus, the integral of E_ρ over the basin south of SR4 transect gives us an indication of the negative buoyancy sources, possibly attributed to deep convection. The corresponding cooling rate computed as an average of E_ρ under the above mentioned 'salt balance assumptions' is found to be 6 W m^{-2}.

Our estimate of the annual mean cooling rate in the area enclosed by SR4 and Antarctica is 22 W m^{-2} which is similar to the 19 W m^{-2} obtained by Fahrbach *et al*., (1994). The model outcome reconciliates the discrepancy between the weak fluxes of Robertson *et al*., (1995) and the ones of Fahrbach *et al*. as a result of intense cooling on the Filchner/Ronne shelf.

Discussion

The employed diagnostic model is formulated as an inverse problem, weakly constrained with respect to the sea surface elevation and buoyancy fluxes. In contrast to traditional strong constraint closures which utilize high-order differential relations for ζ, we solve the problem implicitly, evenly distributing uncertainties in the input fields between the degrees of freedom of the model. Being applied to data sets of a complicated basin, the model has shown a reasonable performance. Spatially varying covariance matrices and transport constraints can also be treated as relatively new elements in the formulation of the model's statistical background. As a rule, climatic hydrological atlases do not contain information on the structure of boundary currents, which are usually confined to the continental slopes and give major contribution to the budgets of various sea water properties. Results of our study show that taking into the account prior information on the spatial variability of the sub-grid processes statistics, one may considerably improve the resolution properties of the optimal state. Prior estimates of the transports, especially

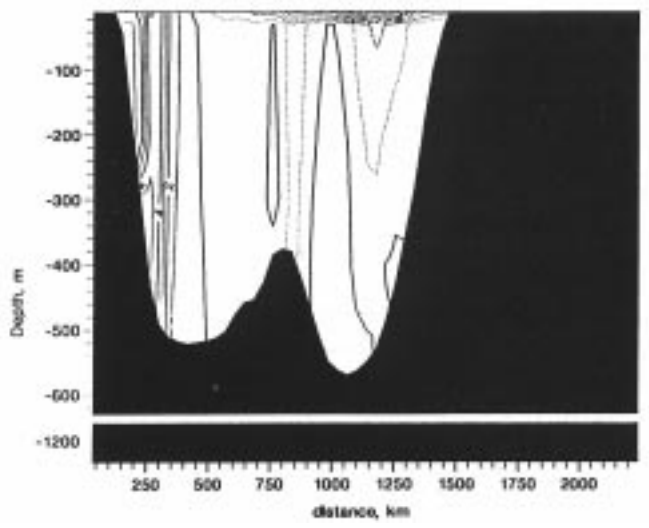

Figure 3. Inverse solution of the cross section velocity (cms^{-1}) at the southern boundary separating the Filchner/Ronne Shelf from the Weddell Sea. The southward flow is concentrated in a shallow surface layer while the return flow is confined to the western slope of the continent.

in the coastal regions also enables the model to refine its structure, bringing the resultant circulation pattern 'closer to nature'.

An obvious drawback of the model is its failure to describe deep convection explicitly. Ocean cooling proves to be hardly observable in oceanic climatologies under standard parametrization of the sub-grid fluxes in the vertical. We expect that including a convective adjustment may partly improve the situation. Problems may arise, however, connected with a rapid loss of information in the vertical coordinate, induced by 'vertical adjustment operators' commonly used in large scale modelling. Adequate non-local parametrizations of the deep convection impact on climatology may be an alternative to improve the situation.

Work is under way to formulate the model for temperature and salinity instead of density. Local refinements of the computational grid are planned as well as using the hydrographic data directly (*i.e.* without gridding them first).

References

Fahrbach, E., G. Rohardt, M.Schröder and V. Strass, 1994: Transport and structure of the Weddell Gyre. Ann. Geophys., 12, 840–855.

Olbers, D., V. Gouretsky, G. Seiβ and J. Schröter, 1992: Hydrographic Atlas of the Southern Ocean. Alfred-Wegener Institut für Polar und Meeresforschung, Bremerhaven, Germany, 19pp., 82 plates.

Robertson, R., L. Padman and M. Levine, 1995: Fine structure, micro structure, and vertical mixing processes in the upper ocean in the western Weddell Sea. J. Geophys. Res., 100, 18,517–18,535.

Yaremchuk, M.I., Nechaev, D.A. and J. Schröter, 1995: A variational analysis of WOCE repeat section SR4. International WOCE Newsletter No. 21.

A Variational Analysis of WOCE Repeat Section SR4

M.I. Yaremchuk, D.A. Nechaev, and J. Schröter, Alfred-Wegener-Institute for Polar and Marine Research, 27515 Bremerhaven, Germany

Traditional concepts used for the analysis of hydrographic sections, *i.e.* geostrophy, conservation of planetary vorticity, hydrostatics,..., are combined with advective balances of active and passive tracers. Additionally to the estimation of velocities across the section this new scheme allows the calculation of vertical and along-section velocities.

Different types of data collected on three cruises from 1989 to 1992 on repeat section SR4 across the Weddell Sea gyre by the Alfred-Wegener-Institute for Polar and Marine Research are integrated into a dynamically consistent pattern of the steady state oceanic circulation using an inverse technique. The data set contains 150 profiles of temperature, salinity and six passive tracers (oxygen, silicate, nitrate, phosphate, ammonium and carbon dioxide) distributed along the section, 53 long current meter records at various points in the transect plane and the large-scale wind stress component taken from the European Centre for Medium Range Weather Forecast data base. The section data are spatially confined to a thin strip of the Weddell Sea body stretching from Kapp Norvegia to the northern tip of Antarctic Peninsula, approximately 40 km wide and 2100 km long. A detailed description of the hydrographic and mooring data is given by Fahrbach *et al.* (1994, 1995).

Inverse solution

We employ a standard variational data assimilation technique. The model has a regular mesh with homogeneous spacing of 35 km in horizontal and uneven spacing in the vertical. There are 62 grid points along the section line, 2 points across and 19 levels. The vertical section defined by the hydrographic data passes through the centres of the grid cells. Tracer data are to be estimated on the grid points, *i.e.* on both sides of the section plane. By this we can calculate not only the mean tracer value (which should be close to the measurement) but also its cross-section gradients. Our inverse problem is obviously underdetermined. In

Table 1. Transport estimates

Data set	V, Sv	T, 10^{12}W	S, 10^{4}kg/s	O_2, 10^{3}M/s	Silicate, 10^{3}M/s	Nitrate, 10^{2}M/s	Phosphate, 10 M/s	Ammonium, 10 M/s	CO_2, 10 M/s
1989	32±4	-35±12	51±35	24±58	138±79	35±62	36±58	62±48	-
1990	32±5	-34±14	52±42	52±51	110±77	13±81	76±72	31±54	-
1992	35±4	-22±10	73±38	84±52	75±68	77±67	160±52	-	74±87
89–92	34±2	-28±8	72±26	45±49	95±66	21±58	180±47	-	-
89–90*	29±9	-35±10	10±22	-	-	-	-	-	-

*Estimates made by Fahrbach *et al.*, 1994

order to find a unique solution a number of constraints are introduced which are widely used to describe the large-scale circulation. These relationships must be satisfied exactly and include geostrophy, hydrostatics and a nonlinear equation of state for sea water. Additionally the linearized potential vorticity balance and advective tracer balances are assumed to be in steady state. Finally an integral constraint imposes no net mass transport across the section. The last three of these constraints are called 'weak', *i.e*. they are to be satisfied only within certain errors bounds defined by *a priori* statistical assumptions.

Table 2. Water mass transformation south of the transect/area of section plane occupied by watermasses

Data set	WDW, Sv	WSDW, Sv	WSBW, Sv	SW, Sv	WDW, %	WSDW, %	WSBW, %	SW, %
1989	-4.6±1.5	2.2±1.7	2.1±2.0	0.3±2.4	23.2	65.1	6.5	5.2
1990	-5.1±1.8	0.9±2.0	2.8±2.2	1.2±2.7	23.3	63.2	8.5	5.0
1992	-3.9±1.5	1.5±1.6	2.2±2.1	0.1±2.5	23.7	65.0	6.4	4.9
89–92	-6.6±1.1	2.6±1.3	2.5±1.9	1.5±2.0	24.3	63.1	7.5	5.1
90*	-6.0	1.2	2.6	2.2	25.6	63.3	6.1	4.9

*Estimates made by Fahrbach *et* al., 1994

The optimal state is obtained via minimization of a quadratic cost function which penalizes model-data misfits, errors in the weak constraints and enforces smoothness in the gridded fields of tracers, horizontal velocities and errors in the tracer advective balance equations. To drive the interpolation pattern away from hydrostatically unstable states the cost function is augmented with an exponential term which penalizes states with unstable profiles and plays the role of a 'range constraint' in continuous form (Schröter and Wunsch, 1986). The model starts from a first guess where tracer values on both sides of the section are equal to the data and with zero velocity at the bottom. In order to close the tracer balances which are dominated by vertical advection in the first guess we have to estimate cross section gradients of tracers which lead to geostrophically balanced along-section velocities. A more detailed description and verification of the assimilation scheme can be found in Nechaev and Yaremchuk (1995).

Estimation of variance has been added as a new aspect to the inverse solution. Error bars for any quantity of interest can be computed through a linear transformation of the covariances between the control variables. The latter are expressed in terms of the inverse of the Hessian matrix *H* associated with the assimilation scheme. This part of the computations turned out to be the most expensive. One single error estimate took about three hours on a Cray YMP/EL which is more than the time necessary to compute the inverse solution itself.

Steady state features of the Weddell gyre

To obtain a better idea of how well the steady state may be estimated from the data, we conducted four assimilation experiments by processing first the available tracer data separately for 1989, 1990 and 1992 and in composition for the 'joint' tracer data set. Major results of these experiments are summarized in Tables 1 and 2.

As an example the assimilated temperature field for 1989 is shown along the section in Fig. 1. Warm Deep Water enters the Weddell Sea in the east whereas the outflow of Weddell Sea Deep Water in the west is confined to the slope of the Antarctic Peninsula.

Net cross-section transports were computed by inte-

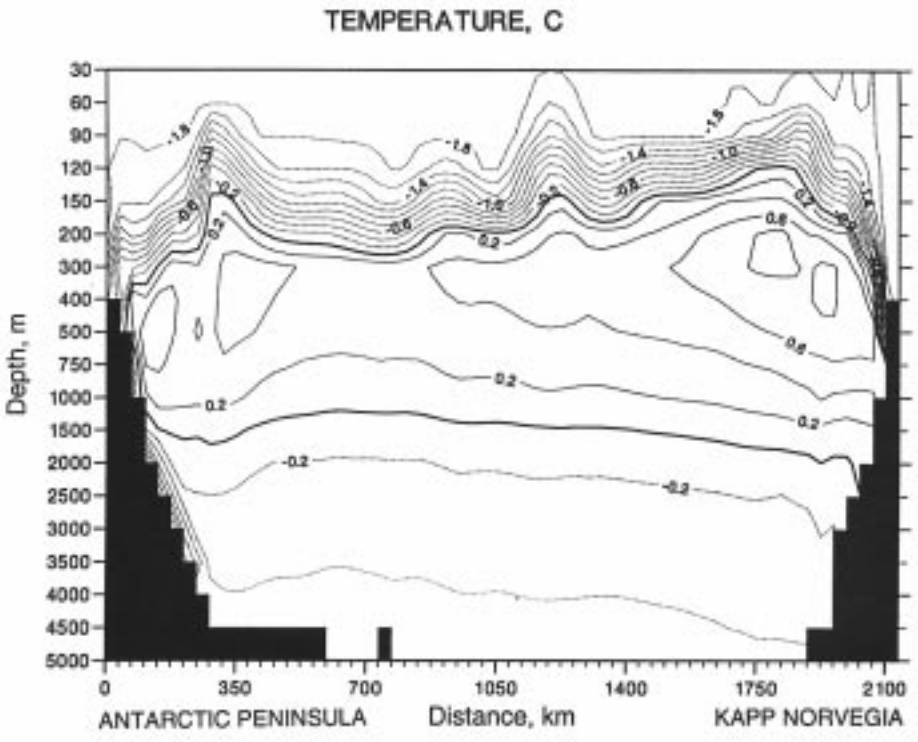

Figure 1. Assimilated temperature field in the SR4 section for 1989.

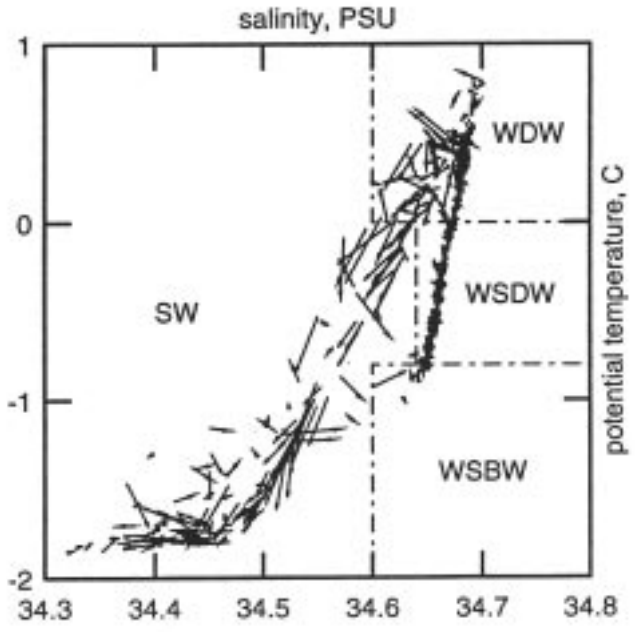

Figure 2. A 'vector' T–S diagram derived from the assimilation solution. Arrows denote annual mean displacements of water parcels in the absence of advection.

gration of the corresponding steady-state fields. Values for most of the transport estimates for tracers and for the water mass transformation rates are much larger than the 70% Gaussian confidence limits. These values may be considered as statistically reliable. It should be stressed that 'reliability' in the sense of the computed error bars is entirely defined by the prior statistical assumptions outlined by the cost function. An idea about the reliability of these hypothesis can be obtained from the variability of the estimates from one data set to another.

On the average the net transport of the Weddell gyre is in agreement with the estimate of Fahrbach *et al*., (1994) ranging between 32–35 Sv. These estimates correspond to a posterior rms discrepancy with velocity measurements of 0.5–1.2 cm s^{-1}. The transport value of 34 Sv from the 'joint' data set was used in a different assimilation study to constrain a three dimensional inverse model of the Weddell Sea (Nechaev *et al.*, 1995).

To study the importance of the current meter measurements for the estimation of the gyre transport Φ we performed a separate assimilation experiment. We decreased the relative weight of the current meter data in the cost function and obtained a net transport of 18–25 Sv. However, the velocity error level was 2–3 cm s^{-1} which seems to be too high for such long-term measurements. From this experiment we have to conclude that the current measurements are very important for the estimation of the gyre transport. Lack of such data leads to high uncertainties in the value of Φ.

Heat transports demonstrate high stability between different data sets, ranging within 22–35 10^{12}W. Dividing this value by the sea surface area south of the transect we get 12–18 W m^{-2} as an estimate for the mean cooling rate in the Weddell Sea. This value agrees rather well with the 16 W m^{-2} derived by Gordon and Huber (1990).

Results for salt transports show a statistically significant salt outflow of $\Phi(S)$=5–7 10^5 kg s^{-1}. However, there should be no net transport of salt in a steady state balance. We may attribute this discrepancy to sea ice which is not included in our model. Both volume and salt can be conserved if we allow a corresponding ice export. Assuming an average salinity for sea ice of 5 psu we interpret the salt flux as a net ice transport of 530 km^3 yr^{-1}. Transports of passive tracers are calculated in Mol per second and shown in Table 1. Although their variances are rather large they support the view that water in the Weddell Sea is enriched by oxygen and biogenic material.

Water mass formation rates shown in Table 2 are derived from the optimal state using a standard technique. Following Fahrbach *et al*. (1994) we divide the section area into four subdomains occupied by different water masses: Surface Water (SW), Warm Deep Water (WDW), Weddell Sea Deep Water (WSDW) and Weddell Sea Bottom Water (WSBW). These water masses are identified by their characteristics in T–S-space (see Fig. 2). The last four columns in Table 2 demonstrate the relative contributions of these domains to the area of the section plane. Integrating the cross section velocities over these subdomains, we obtain an idea of the net water mass transformation rate in the Weddell Sea south of the transect. The composed data indicate that inflow of the WDW splits into outflows of WSDW and WSBW which are almost equal. The contribution of the SW in this diagram appears to be statistically uncertain.

The advective tracer balances are solved in a least squares sense. Small discrepancies remain after the assimilation. They have the dimension of time derivatives. To study these trends they were integrated for one year and plotted as arrows in a T–S-diagram (Fig. 2). Each arrow starts at assimilated T–S values and points at the respective values one year later. After the minimization residuals should in general be randomly distributed. In our case it is remarkable how much the residual trends resemble mixing of watermasses and describe a process that is not modelled explicitly.

Summary

Major results of the assimilation are:

1. The Weddell gyre transports water at the average rate of 34±2 Sv.
2. Heat is transported poleward at the rate of 28±8 10^{12} W which translates into 15±3 W m^{-2} as an estimate of the annual mean cooling rate of the Weddell Sea south of the transect.
3. Salt transport estimates give an indication of a net ice outflow from the Weddell Sea of 530±250 km^3 yr^{-1}.
4. Passive tracers (oxygen, silicate, nitrate, phosphate, ammonium and carbon dioxide) are transported out of the Weddell Sea at rates of $45 \pm 49 \cdot 10^3$, $95 \pm 66 \cdot 10^3$, $21 \pm 58 \cdot 10^2$, 1800±470, 470±510 and

740±870 Mol s^{-1} respectively.

5. Processes occurring south of the section transform 6.6±1.1 Sv of the inflowing Warm Deep Water into approximately equal amounts of Weddell Sea Deep Water and Weddell Sea Bottom Water. Surface Water seems to play a minor role. This is in contrast to Fahrbach *et al.* (1994) who estimate a significantly smaller transport of WSDW and higher transports of SW from the same data set.

The type of analysis described here can be used for other WOCE sections. In our solution the current measurements constrained the solution quite strongly. For other areas we may therefore suggest that either current meter velocities or other independent data like satellite altimetry should be used in order to estimate transports that are statistically reliable.

References

Fahrbach, E., G. Rohardt, M. Schröder and V. Strass, 1994: Transport and structure of the Weddell Gyre. Ann. Geophys., 12, 840–855.

Fahrbach, E., G. Rohardt, M. Schröder, and V. Strass, 1995: Weddell gyre study 1989–1993. WOCE Newsletter, No 18.

Gordon, A.L., and B.A. Huber, 1990: Southern Ocean winter mixed layer. J. Geopys. Res., 95, 11655–11672.

Nechaev, D.A., M.I. Yaremchuk, and J. Schröter, 1995: A steady state inverse model of the large scale circulation of the Weddell Sea. WOCE Newsletter, this issue.

Nechaev, D.A., and M.I. Yaremchuk, 1995: Application of the adjoint technique to processing of a standard section dataset: World Ocean Circulation Experiment section S4 along 67°S in the Pacific Ocean. J. Geophys. Res., 100, 865–879.

Schröter, J., and C. Wunsch, 1986: Solution of non-linear finite-difference open ocean models by optimization method with sensitivity and observational strategy analysis. J. Phys. Oceanogr., 16, 1855–1875.

NE Atlantic Circulation and Fluxes From CONVEX 1991

Sheldon Bacon, Southampton Oceanography Centre, Empress Dock, Southampton, SO14 3ZH, UK

CONVEX (Control Volume Experiment) was designed as a hydrographic survey of the interior of the Sub-Polar Gyre of the North Atlantic (including AR12 and AR7E of the WOCE Hydrographic Programme). The cruise took place between 1 August and 4 September 1991 on the RRS Charles Darwin, between the European continental shelf off Ireland and Cape Farewell, Greenland. The cruise programme is described in Gould (1992), station positions and bathymetry are shown in Fig. 1. A total of 96 stations were occupied. CTD data were collected using an NBIS Mark 3b instument. ADCP data were recorded continuously from stations 5 to 95; the data processing is described in Hartman (1992). Previous results relating to climate change are described in Read and Gould (1992), and relating to hydrographic inverse methods in Bacon (1994).

The first matter which had to be tackled before making any attempt to calculate property fluxes or estimate circulation schemes was the 'absence' of the East Greenland Current (EGC) from the data. Particularly foul and unseasonable weather by Greenland stopped the CTD sections just short (by about 15 km) of the EGC, and about 70 km from the Greenland coast. We decided to construct a hybrid EGC therefore, using historical data to provide property profiles and geostrophic shear, and the most appropriate data for this were stations taken by the RV Anton Dohrn in 1958 as part of the International Geophysical Year (IGY) work, which fitted to the western end of the southern CONVEX section. As can be seen from Fig. 2, the Darwin spent a considerable amount of time hove-to within the EGC, in the course of which a few days' good ADCP data (low ship speed) were recorded and used to estimate the barotropic element of the EGC. Finally, overlapping stations between CONVEX and the IGY data were used to calculate adjustments to the property profiles on account of climate changes since 1958.

Given a complete data set, we were then able to proceed with the generation of a flow field. We use an inverse method to estimate the geostrophic reference currents, so we arrive at a 'first guess' state to input to the inversion by finding the level of no motion which produces minimum flow divergence. This level is at σ_2 = 36.93, which is near the middle of the Labrador Sea Water layer. Then we run the inversion several times, with different constraints, different layers and different solution endpoints so we have some idea of the range of feasible solutions. The principal constraint, to which all solutions are forced, is that net volume flux across the section should equal zero. This

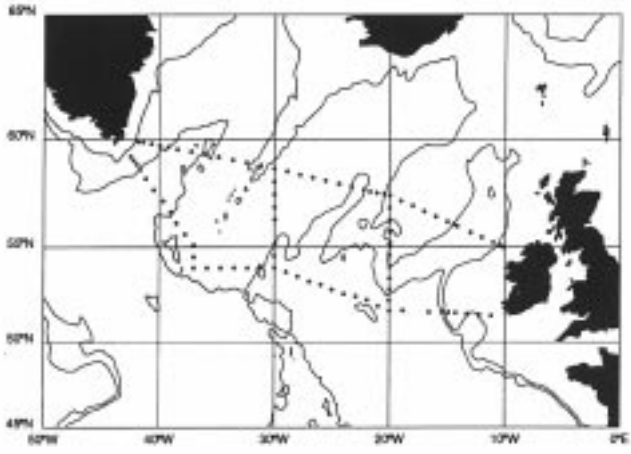

Figure 1. CONVEX station positions. Topography is illustrated with 1500 m and 3000 m depth contours.

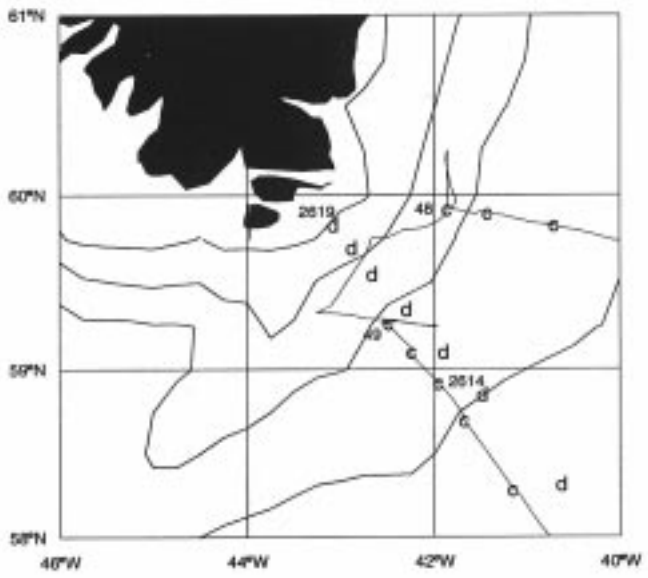

Figure 2. Magnified view of the western end of the CONVEX area at Cape Farewell. Letter 'c' indicates CONVEX station positions (as Fig. 1), letter 'd' indicates RV Anton Dohrn station positions. The six of these latter employed in the analysis are numbers 2614 (south-eastern) to 2619 (north-western). The continuous line joining the CONVEX stations is the track of the RRS Charles Darwin. Depth contours shown are 200, 1000, 2000 and 3000 m. The eastern edge of the EGC lies just west of stations 48 and 49, determined from surface salinity measurements (not shown).

includes Ekman fluxes, estimated from Hellerman and Rosenstein (1983) climatology. It is probably correct to ±1 Sv (1 Sv = 10^6 m^3s^{-1}), since the inflow to the Arctic at the Bering Straits is about 1 Sv (Roach *et al.*, 1995), the Canadian Archipelago throughflow is between 0 and 2 Sv (Bacon, 1995, and references therein), and the net Arctic freshwater gain is small, O(0.1 Sv).

Having arrived at a working model of the circulation, we then compare it with existing circulation schemes and it holds up quite well, with the major obvious exception of the Denmark Strait Overflow (DSO). Our scheme has the DSO very weak compared, for example, to Clarke (1984): 3–4 Sv as against 13 Sv. More detailed comparison of CONVEX and Clarke shows that our deep shear is weaker than both his and than the IGY data by about 5 Sv, but also that we probably do not have the geostrophic reference currents correct just east of the EGC. The current regime on-shelf and on the shelf edge is quite complicated. Inshore there is the EGC, whose eastern edge is marked by a sharp salinity front. East of this are the Irminger Current (IC) in the upper ocean and the DSO near the bottom. In trying to get the flows correct over this regime, we are trying to untangle the effects of (1) long-term (climate) variability, (2) short-term (days-weeks-months) variability and (3) inadequate constraints/measurements. We discuss these matters in greater detail elsewhere (Bacon, 1995); here, we will give a brief summary of how we arrive at our preferred solution.

We have so far treated the western boundary current (WBC) as the EGC alone, *i.e.*, from the coast to the sharp salinity front marking the eastern edge of the EGC. The work of Clarke (1984) has suggested that there are still significant currents at the density level corresponding to the level of no motion, and also therefore no current zero in the water column, continuing some way east of this, associated with the Irminger Current flowing south immediately adjacent to and 'outside' the EGC. This may extend a further 100 km or so offshore, with an abrupt current reduction at its eastern edge. We do not have enough CONVEX ADCP data to estimate the reference current with much confidence here, so we treat it as a parameter and see how it is bounded. The IC lies over our 'weak' DSO, so without changing the deep shear, we cannot increase the barotropic currents much, to increase the DSO, before we arrive at historically unrealistic values of the Sub-Polar net circulation. To get 13 Sv in the DSO by barotropic adjustment would require, for example, 60 Sv in the whole Sub-Polar gyre, which is nearly double typical previous estimates.

Now in treating the barotropic flows immediately east of the EGC as a parameter, we apply these adjustments to our best, balanced (zero net volume flux) flow scheme between Greenland and Ireland. We must retain the balance by redistributing this extra flux elsewhere, and we choose to do this by sending it northwards in the North Atlantic Current on the shelf edge immediately west of the Rockall-Hatton Plateau, where van Aken and de Boer (1995) have measured a northwards current of about the 'right' magnitude at the depth of the 'level of no motion'. We illustrate the results of this with vertically-integrated fluxes of volume, temperature and salinity in Fig. 3 for the CONVEX south

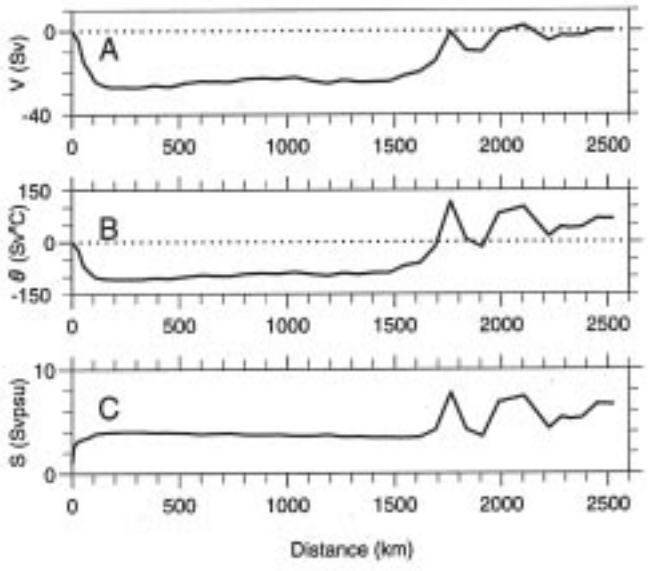

Figure 3. Depth-integrated transport for the CONVEX south section, accumulated from zero at the west (left), of (A) volume (V, Sv), (B) potential temperature (θ, Sv°C) and (C) salt (S, Svpsu). Net property flux for the section appears in the eastermost point (the furthest to the right). The dotted line is that of zero flux, for reference.

section, accumulated eastwards from zero at the west end of the section. One can see there that southward flows are concentrated in the west in a narrow, 100 km-wide band, and that the balancing northward return flows in the east are wider, covering over 1000 km, and contain much eddy energy. The salt flux is dominated by southward fresh fluxes and northward saline fluxes, both near the surface. Heat fluxes are more three-dimensional, with southward cold flow at depth and warm northward surface flow.

After running various sensitivity tests, we concluded with (for zero net mass flux) a net heat flux of 0.28±0.08 PW polewards, and a net salt flux of 6.5±1.6 Svpsu (1 Sv = 10^6 m^3s^{-1} psu = practical salinity unit) polewards. Within the stated errors, we were unable to discern any significant difference between net fluxes across the CONVEX north and south sections, so we refer to fluxes 'across the CONVEX region', and ascribe a nominal latitude of 55˚N to these estimates. The heat flux is about right when compared, for example, with the Isemer *et al.* (1989) reanalysis of the Bunker heat fluxes. With the aid of various other constraints, we were able to convert the salt flux into an estimate of the net freshwater gain of the whole Arctic Basin, which came out at 0.17 Sv. This is similar to previous direct and indirect estimates, which lie in the range 0.1–0.2 Sv. One interesting consequence of the present calculations is that nearly half of the Arctic freshwater gain is exported *on-shelf* by the EGC.

References

van Aken, H.M., and C.J. de Boer, 1995: On the synoptic hydrography of intermediate and deep water masses in the Iceland Basin. Deep-Sea Res., 42 (2) 165–189.

Bacon, S., 1994: Skill in an inversion solution: CONVEX-91 hydrographic results compared with ADCP measurements. J. Atmos. Oceanic. Tech. 11 (6) 1569–1591.

Bacon, S., 1995: Circulation and fluxes in the North Atlantic between Greenland and Ireland. J. Phys. Oceanogr., submitted.

Clarke, R.A., 1984: Transport through the Cape Farewell–Flemish Cap section. Rapp. P.-v. Réun. Cons. int. Explor. Mer, 185 120–30.

Gould, W.J., 1992: RRS Charles Darwin Cruise 62 1 August – 4 September 1991. CONVEX - WOCE Control Volume AR12. IOSDL Cruise Report No. 230, 60 pp.

Hartman, M.C., 1992: Shipboard ADCP observations during RRS Charles Darwin Cruise 62. IOSDL Report No. 298, 27pp.

Hellerman, S., and M. Rosenstein, 1983: Normal monthly wind stress over the world ocean with error estimates. J. Phys. Oceanogr., 13 (7) 1093–1104.

Isemer, H-J., J. Willebrand and L. Hasse, 1989: Fine adjustment of large-scale air-sea energy flux parameterisations by direct estimates of ocean heat transport. J. Climate, 2 (10) 1173–184.

Read, J.F., and W.J. Gould, 1992: Cooling and freshening of the subpolar North Atlantic Ocean since the 1960s. Nature, 360 (6399) 55–57.

Roach, A.T., K. Aagaard, C.H. Pease, S.A. Salo, T. Weingartner, V. Pavlov and M. Kulakov, 1995: Direct measurements of transport and water properties through the Bering Strait. J. Geophys. Res., 100 (C9) 18443–18457.

Drifter Measurements in the Nordic and Barents Seas

P.-M. Poulain, SACLANTCEN Undersea Research Centre, La Spezia, Italy

107 Argos tracked drifters were released in the Nordic Seas (or Greenland, Iceland and Norwegian Seas) from June 1991 to August 1993 to measure the spatial and temporal variabilities of the near surface currents and of the Sea Surface Temperature (SST).

Drifters were deployed from various research vessels and volunteer observing ships in three main regions: east of Iceland, on the Norwegian shelf and in the Greenland basin. The drifter used was the WOCE/TOGA Lagrangian drifter with a holey-sock drogue centred at 15 m depth fitted with a thermistor to measure SST, and two drogue-presence sensors (sea-water switch and strain gauge). In the harsh environment of the Nordic Seas, the half-lives of the Argos transmitter, the attached drogue and the thermistor were 190 days, 157 days and 114 days, respectively.

The data set spans the period of June 1991 to April 1995 with a maximum of drifter observations in November 1992. This represents more than 85 years of drifter-days, from which 67% have the drogue attached and 71% have reliable SST measurements. Some of the drifters crossed the 20°E longitude and entered the Barents Sea between northern Norway and Bear Island. The drifter data available in the Barents Sea amounts to 14% (12 drifter-years) of the total data set. Since no deployments were conducted in or near the Barents Sea, most of the drifters which entered the Barents Sea had lost their drogue (56% of undrogued drifter data).

The drifter data cover most of the ice-free Nordic Seas and the southern Barents Sea (Fig. 1). The most interesting circulation features revealed by the drifter trajectories are briefly commented upon hereafter. More details about the drifter data set and its interpretation can be found in a forthcoming paper (Poulain *et al*., 1995).

Basin-wide and sub-basin cyclonic circulation gyres

Drifter tracks are concentrated at the periphery of the Nordic Seas from the Iceland-Faroe Ridge region to Spitsbergen (Fig. 1), corresponding to the southern and eastern rims of a basin-wide cyclonic gyre. This circulation is closed by the southwestward current east of Greenland and by southeastward flow northeast of Iceland (both barely sampled by the drifters due to ice coverage and

inadequate deployment strategy). The concentration of drifter paths into narrow persistent streams (typically 50 km wide) is striking in the Norwegian Atlantic Current system extending from the Iceland-Shetland Ridge to Fram Strait. If the fast drogued drifter displacements with speed >40 cm/s are superimposed on bathymetry (Figs. 2a and 2b), it becomes evident that these narrow streams are relatively rapid and that they follow the continental margins of the Nordic Seas. Other strong mean currents are associated with the strong surface salinity fronts of the Iceland-Faroe Frontal zone and the Norwegian shelf. A closer look at the drifter trajectories in the context of the underlying topographic features indicates that smaller cyclonic circulation patterns exist in all of the major sub-basins, *i.e.*, the Iceland Plateau (IP), the Norwegian (NB), Lofoten (LB) and Greenland (GB) basins (see Fig. 2a for geographical location). These flows follow the slopes around the sub-basins and drifters have a tendency not to cross the ridges separating the basins.

Branching of the Norwegian Atlantic Current

The relatively warm and saline Atlantic water entering the Nordic Seas over the Iceland-Shetland Ridge flows northward as a main central current following the Norwegian shelf break, extending north toward Spitsbergen (West Spitsbergen Current) and east into the Barents Sea (North Cape Current). Between 63°N and 67°N, the drifter tracks show two other persistent streams which are also contributing to the northward transport of Atlantic water. The first is the Norwegian Coastal Current associated with the surface salinity front separating relatively saline Atlantic and fresher Norwegian shelf waters. The second stream lies to the west of the main core on top of the slope (Fig. 2a) between the Voring Plateau (VP, 1500 m) and the Norwegian Basin (NB, 3000 m). This branch separates from the main inflow stream near 63°N–0°E, then continues northeastward before flowing NNW. At 67°N, the major part of that flow recirculates in the Norwegian Basin cyclonic gyre, whereas a small fraction turns eastwards and joins the main stream west of Lofoten Island. Regions of low drifter concentration are evident between these three streams near 64°N indicating that the surface circulation in these areas is probably divergent. Between 68°N and 70°N, the three cores of the Norwegian Atlantic current merge into a single swift current confined on the shelf break off the Lofoten and Vesteralen Islands (Fig. 2b). The strongest measured currents were in excess of 110 cm/s in this confluent flow regime.

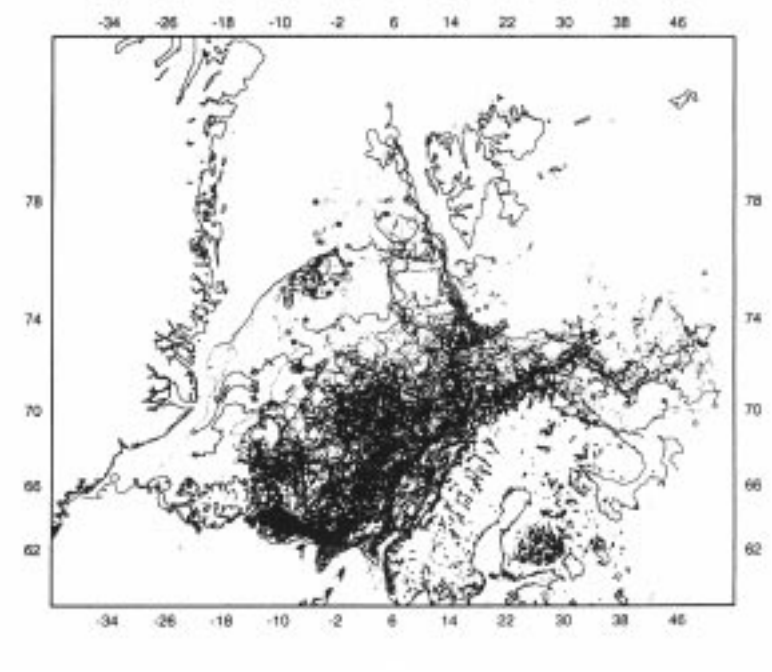

Figure 1. Trajectories of drogued (solid) and undrogued (dotted) surface drifters in the Nordic and Barents Seas in the time period of June 1991 to April 1995. Release and last transmission sites are represented by star and circle symbols, respectively.

High eddy activity in the Lofoten Basin

The major part of the mean surface transport of Atlantic water across, say 70°N, takes place in a narrow stream following the Norwegian shelf break. To the west of this strong flow, the drifter data reveal very little mean circulation and an enhanced eddy activity (15 cm/s r.m.s.) throughout the Lofoten Basin (LB, see Fig. 2a). The contribution of these energetic eddies to the northward transport of Atlantic water has to be quantified and compared to the transport by the mean stream. It is, however, obvious from this new Lagrangian data set that no mean current exists in the Lofoten basin as was demonstrated by historical hydrographic and ship drift observations (Alekseev and Istoshin, 1956). It can be shown that these eddies have a tendency to propagate westward and that they probably originate from baroclinic instabilities of the strong mean Norwegian Atlantic Current (Poulain *et al.*, 1995).

No evidence of surface East Icelandic Current

The drifters released northeast of Iceland in cold, low-salinity modified Arctic waters reveal a quiescent surface circulation, in the mean and eddy field. They had great difficulty crossing the temperature/salinity front to the south and to the east, several meandering in the salinity minimum tongue for more than a year. Most of those which eventually escaped moved onto or near the east Icelandic shelf and joined the Iceland-Faroe Front circulation system. No surface evidence of a significant broad East Icelandic Current expanding off the northeast Icelandic shelf is given by the drifters.

Barents Sea circulation

The surface circulation in the southern Barents Sea as measured by the drifters is dominated by the North Cape Current confined to the north coast of Norway which is an extension of the Norwegian Atlantic Current. Further to the east, this current system appears to move away from the coast near 25°E and meander eastward as far as 45°E (Murman Current) influenced by the underlying topography. Another important feature is the eastward excursion of drifters leaving the West Spitsbergen Current near 73°N. This circulation pattern is associated with the Polar front south of Bear Island. Some drifters recirculated at 23°E, meandered westward and rejoined the West Spitsbergen Current, in good agreement with recent hydrographic and ADCP observations collected in the area (Parsons *et al*., 1995). Others moved eastward and eventually joined the main stream system near 32°E.

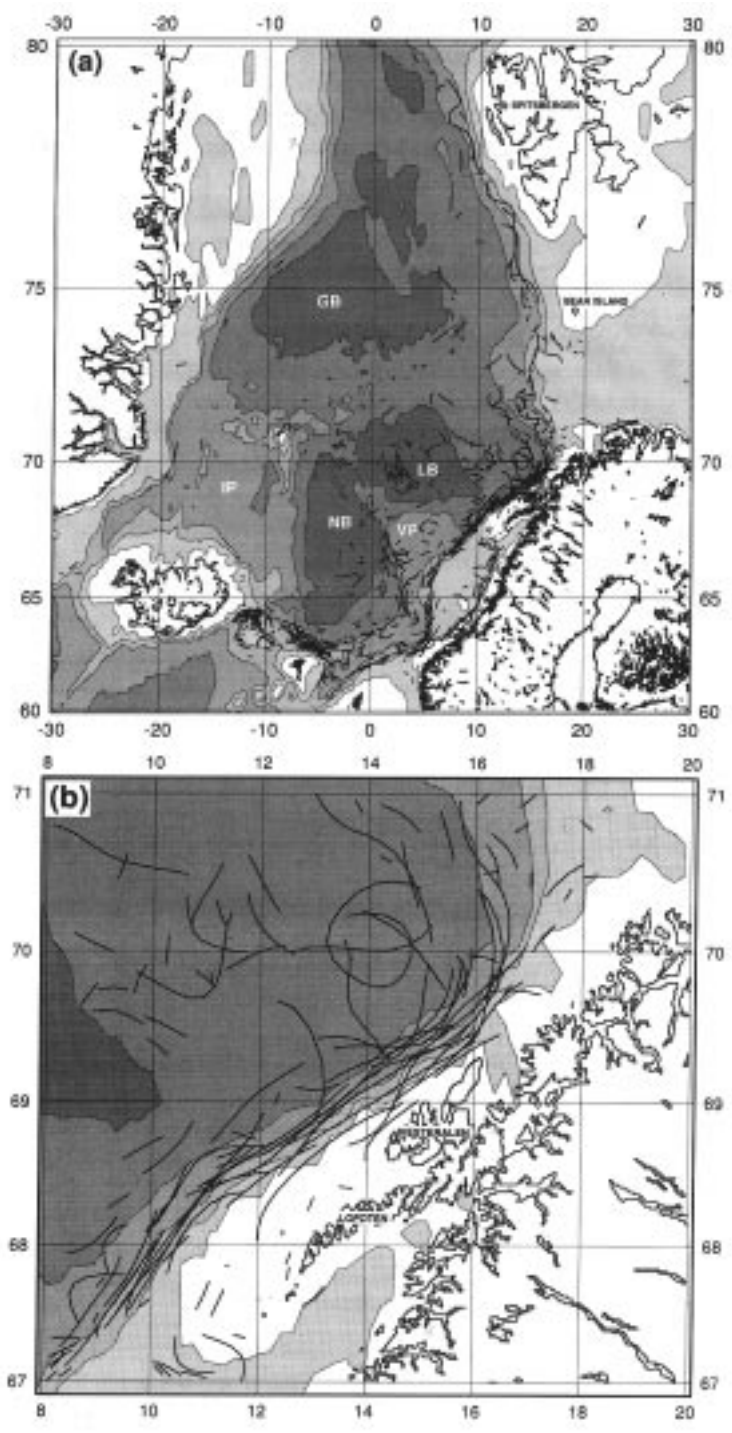

Figure 2. Trajectory segments corresponding to fast currents (>40 cm/s) as measured by drogued drifters. Bathymetry is depicted with gray shades and the names of the major topographic features are posted: Iceland Plateau (IP), Norwegian Basin (NB), Voring Plateau (VP), Lofoten Basin (LB) and Greenland Basin (GB): (a) Nordic Seas, (b) Close-up of the Norwegian Atlantic Current off the Lofoten and Vesteralen Islands.

References

Alekseev, A.P., and B.V. Istoshin, 1956: Chart of constant currents in the Norwegian and Greenland seas. Trans. Knivovich Polar Sci. Inst., 9, 62-68 (in Russian); pp. 69-76 in Special Report, Fisheries, 327, U.S. Dept. Int., Fish and Wildlife Service, Washington, D.C.

Parsons, A.R., R.H. Bourke, R.D. Muench, S.-C. Chiu, J.F. Lynch, J.H. Miller, A.J. Plueddemann, and R. Pawlowicz, 1995: The Barents sea Polar front in Summer. J. Geophys. Res., accepted.

Poulain, P.-M., A. Warn-Varnas and P.P. Niiler, 1995: Near surface circulation of the Nordic Seas as measured by Lagrangian drifters. J. Geophys. Res, accepted.

Second Revision of the WOCE Data Handbook

Originally issued in March 1994, the WOCE Data Handbook has already gone through two revisions with the latest completed December 1995. Revised chapters should be in the hands of all those who received earlier versions in January.

The amount of data arriving at WOCE Data Assembly Centres is increasing as WOCE reaches the point in its field programme where many individual projects have been completed. Also, modifications to data submission and sharing practices are being implemented to accelerate data assembly. As a result, printed data information sources like the Handbook quickly get out-of-date in some respects. That's actually good news, not a complaint, and there are other ways to keep current with WOCE. We urge you to use OCEANIC, the electronic on-line information system, in conjunction with the Handbook as OCEANIC is updated frequently. The latest version of the Handbook emphasizes the many World Wide Web links that exist within components of the WOCE Data System and with other WOCE related data and information sources. For those of you not in a position to utilize OCEANIC and the Web, you may wish to receive the hard copy version of OCEANIC's WOCE Field Programme summary which will be issued next Spring by the Data Information Unit. For information on any of the electronic systems or publications, including requests, contact the DIU via internet: woce.diu@diu.cms.udel.edu, Fax: (1) 302-645-4007, or mail: K. Bouton, College of Marine Studies, University of Delaware, Lewes, DE 19958, USA.

The Handbook will be updated again fall 1996. We welcome feedback on its contents and any field programme or data systems updates that we have missed or PIs wish expanded upon.

Deep Basin Experiment: Meteor Float Missions in the Southern Brazil Basin Successfully Completed

Walter Zenk, Olaf Boebel, and Claudia Schmid, Institut für Meereskunde an der Universität Kiel, 24105 Kiel, Germany

One and a half years ago we reported about the 28th cruise of FS Meteor devoted to WOCE activities in the South Atlantic (WOCE Newsletter, 16). After completion of the basin-wide WHP section A8 on 11°S the Meteor operated in the southern Brazil Basin between 21°S and the Subtropical Convergence on a quasi-meridional section. During this cruise, lasting from 15 May–14 June 1994, intensive mooring work in the region of the Hunter Channel at 34°S was finished, yielding the first direct current observations from this important passage for bottom water exchange between the Argentine Basin and the Brazil Basin (Zenk and Müller, 1995).

A further objective of the oceanographic work on board the Meteor dealt with the observation of Antarctic Intermediate Water (AAIW). This water mass in the Atlantic is traditionally thought to be mainly generated in the southwestern South Atlantic, though admixtures of intermediate waters advected through Drake Passage may play a significant role in its formation. After its subduction north of the polar frontal zone AAIW penetrates northward into subtropical regions. The spreading of AAIW has drawn increasing attention because of its balancing role in large-scale oceanic mass and heat transports. Low-saline and oxygenated AAIW can be found in all three oceans. Its global impact is especially obvious in the Atlantic where AAIW is advected far into the northern subtropical gyre compensating partially the mass deficit caused by the southward flowing North Atlantic Deep Water.

Recognizing the importance of AAIW for the global meridional circulation cell and for the regional hydrography of the Brazil Basin an internationally coordinated float programme with participants from France, Germany, and the USA has been initiated under the auspices of the Deep Basin Experiment in WOCE. While south of the South Atlantic Current ALACE profilers were or are on their missions (Davis *et al*., 1995), in the subtropics and tropics RAFOS and MARVOR (Ollitrault *et al*., 1995) floats were deployed at the level of AAIW, *i.e.* around 800 m depth. The necessary basin-wide insonification for the RAFOS technology (Rossby *et al*., 1986) is provided by a sound source array supplied by laboratories in Brest, Kiel, and Woods Hole.

As part of these efforts the Institut für Meereskunde was engaged in the deployment of 71 RAFOS floats in 1994 on the western side of the South Atlantic. An initial series of 29 launches of the 1994 cluster were performed during Meteor cruise No. 28 (Fig. 1). Previously (December 1992) a shorter experiment with 21 floats had been conducted across the Rio-Grande Rise (Siedler *et al*., 1993) of which 15 instruments returned trajectories. A third batch of 42 RAFOS floats was seeded in October 1994 from FS Polarstern (Boebel and Schmid, 1995). While the latter experiment is still ongoing we are happy to announce that on 20 November 1995 the last Meteor float returned to the surface in due time after an 18 months long mission. Only two floats failed to return to the surface and to transmit data, which results in a success rate of 93%. Virtually all returned floats appear to have performed excellently, as first evaluations of the obtained trajectories show (Fig. 2). The instruments were all built and ballasted at Institut für Meereskunde in Kiel. They contained electronic boards by

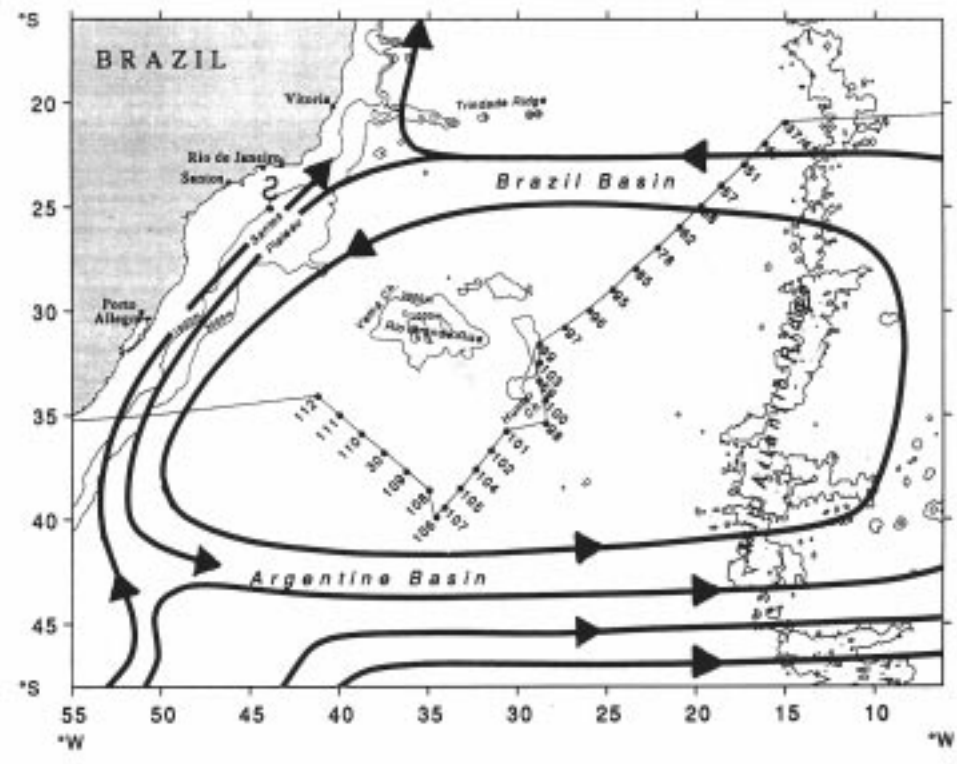

Figure 1. Cruise track of Meteor cruise No. 28. Dots denote RAFOS launch sites at a nominal distance of 1 degree latitude. A cartoon of the general circulation of Antarctic Intermediate Water according to Warren and Weiss (1992) has been superimposed.

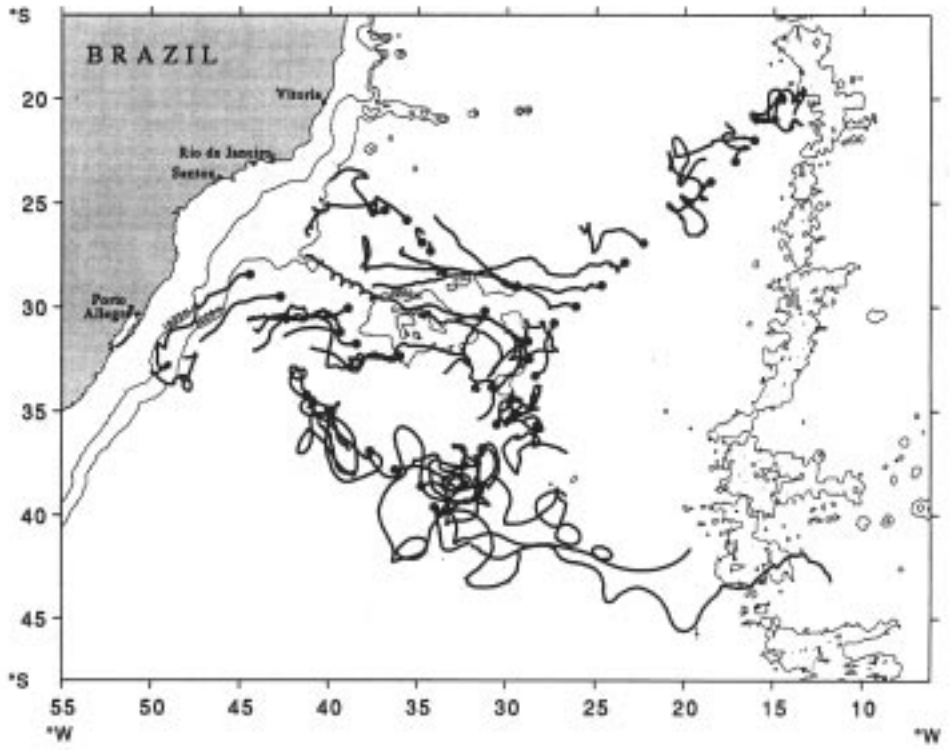

Figure 2. 29 RAFOS floats were launched during Meteor cruise 28 (•). The figure shows all available trajectories from this and the preceding shorter experiment during Meteor cruise 22 in December 1992. Mission lengths varied between 3 and 18 months. The farthest float received signals over a distance of >3000 km.

Bathy Systems, Inc. The floats hit their target depths within ±10 dbar. The Meteor 28 data set consists of approximately 9180 float days or roughly 25 float years.

Single trajectories of different mission lengths in Fig. 2 must be discussed with great caution. Nevertheless, a first inspection of the obtained pathways shows a high degree of consistency with the circulation scheme proposed by Warner and Weiss (1992) for the South Atlantic. After the main bulk of AAIW on its equatorward drift on the western slopes of the Argentine Basin approaches the Subtropical Convergence Zone it is captured by the merging process of the Falkland/Malvinas Current and the Brazil Current, and is advected with the deep South Atlantic Current eastward (Fig. 1). Off the African con-

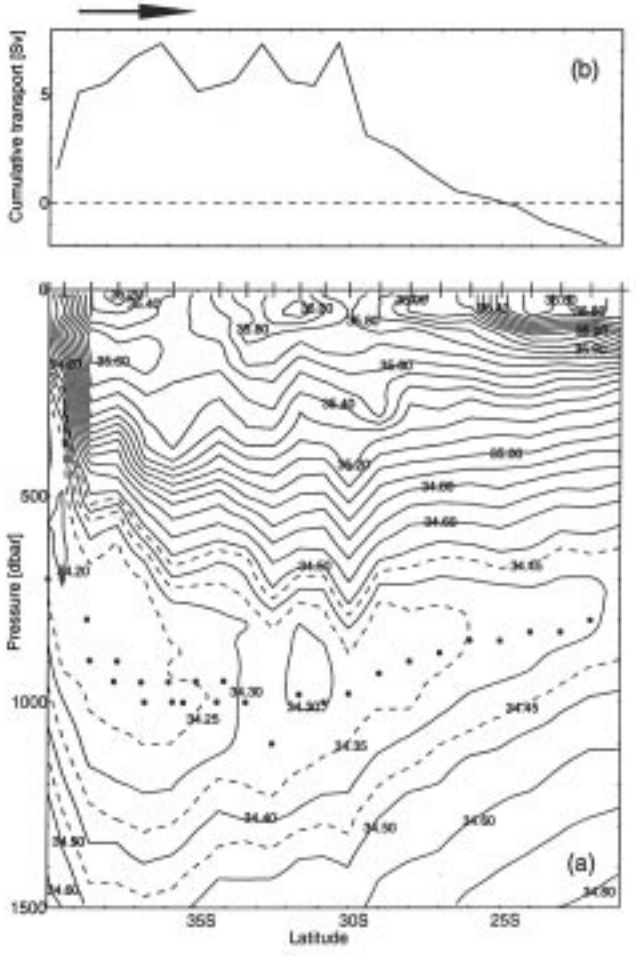

Figure 3. Salinity distribution (a) in the upper 1500 dbar during Meteor cruise 28 in May 1994. For location see Fig. 1. Note the low saline core layer (S<34.40) of Antarctic Intermediate Water (AAIW) at approximately 800 m. At the southern side (left) the Subtropical Convergence is clearly recognizable. 21 out of 29 RAFOS floats (•) were launched in the core layer of AAIW shown as the long section in Fig. 1. All floats were individually ballasted to reach the salinity minimum layer according to pre-launch CTD soundings. Part (b) shows the integrated geostrophic transport of the subtropical circulation cell of AAIW between 500 and 1200 dbar relative to σ_1 = 32.1 kg m^{-3}. The centre of the subtropical gyre appears to lie roughly at 30–35°S, i.e. at the latitude of the Rio-Grande-Rise.

Acknowledgement

Our RAFOS float work in the depth level of the Antarctic Intermediate Water of the South Atlantic was funded by contracts 03F0121A and 03F0157A from the Bundesminister für Bildung, Wissenschaft, Forschung und Technologie, Bonn.

tinent one expects a flow divergence. The return flow of the AAIW remains in the South Atlantic whereas the rest reaches the Indian Ocean (Shannon and Hunter, 1988). The westward part is influenced by the Agulhas Extension Current regime and the Benguela Current. After the AAIW crosses zonally once again the Mid-Atlantic Ridge it reaches the great bight off Rio de Janeiro, where one expects another divergence region for AAIW. Partially the AAIW flows northward as a boundary current on the Brazilian slopes, partially the AAIW closes a recirculation loop. In Fig. 3a we display the bowl-shaped distribution of low-saline AAIW cutting through the recirculation cell in the subtropics. Estimates of geostrophic transports (Fig. 3b) indicate $8 \cdot 10^6\,m^3s^{-1}$ rotating anticyclonically in the basin-wide cell of the AAIW. Further investigation of this phenomenon on the eastern side of the subtropical South Atlantic is planned with more RAFOS floats around southern Africa for 1997.

References

Boebel, O., and C. Schmid, 1995: RAFOS floats in the South Atlantic. Ber. Polarforschg., Bremerhaven, 168, 6–11.

Davis, R.E., P.D. Killworth and J.R. Blundell, 1995: Comparison of ALACE and FRAM results in the Southern Atlantic. J. Geophys. Res. (submitted).

Ollitrault, M., Y. Auffret, N. Corths and J.P. Rannon, 1995: The SAMBA Experiment. Ber. Polarforschg, Bremerhaven, 168, 11–18.

Rossby, T., D. Dorson and J. Fontain, 1986: The RAFOS System. J. Atm. Oc. Tech., 3, 672–679.

Shannon, L.V., and D. Hunter, 1988: Notes on Antarctic Intermediate Water around Southern Africa. S. Afr. J. Mar. Sci., 6, 107–117.

Siedler, G., W. Balzer, T.J. Müller, R. Onken, M. Rhein and W. Zenk, 1993: WOCE South Atlantic 1992, Cruise No. 22, 22 September 1992–31 January 1993. Meteor-Berichte, Universität Hamburg, 93–5, 131 S.

Warner, M.J. and R.F. Weiss, 1992. Chlorofluoromethanes in South Atlantic. Deep-Sea Res., 34, 2053-2075.

Zenk, W. and T.J. Müller, 1995. WOCE Studies in the South Atlantic, Cruise No. 28, 29 March–14 June 1994. Meteor-Berichte, Universität Hamburg, 95-1, 193 pp.

Subsurface Float Data

P.L. Richardson and C.M. Wooding, Woods Hole Oceanographic Institution, Woods Hole, MA 02543, USA

The purpose of this note is to show summary plots and tables of assembled float data so that WOCE scientists can see the available data and learn how to acquire them. The WOCE subsurface float data assembly center (WFDAC) has assembled pre-1990 float data and more recent data which are presently available. These float data have been submitted to the National Oceanographic Data Center (NODC) – World Data Center A (WDC-A) where they are available to scientists worldwide. The data were recently (August 1995) released by NODC in a CD-ROM entitled CD-ROM NODC-53, Disc 1, Subsurface Float Data, Surface Current (Ship Drift) Data. Presently available are approximately 500 float trajectories and 450 float-years of data (Fig. 1, Table I). Float depths range from a few hundred metres to several thousand, with most observations falling in the 700–2000 m depth range. Most of the trajectories are located in the North Atlantic and were obtained as part of various experiments during 1972–1992.

Figure 1. Pre-1990 neutrally buoyant float data held at the WOCE data archive.

Table I: Summary of Available Float Data Assembled by the WFDAC (November 1, 1995)

Institution	Source/PI	Experiment Identifier	Location	Years	# of Floats	Type	Nominal Depth (m)	Ave. Duration (days)	Float Yrs
URI	Rossby	MO	28°N, 70°W	1972–76	47	SOFAR	1500	178	22.9
NAVOCEAN/WHOI	Cheney/Richardson	RI	33°N, 70°W	1974–75	8	SOFAR	1100	154	3.4
URI	Rossby	PL	20–30°N, 55–75°W	1975–79	20	SOFAR	700, 2000	586	32.1
URI	Rossby	LD	31°N, 70°W	1978–79	45	SOFAR	700, 1300	164	20.2
WHOI/URI	S, P, R, O, R	LR/GS	36°N, 65°W	1978–79	5	SOFAR	700, 1300, 2000	316	4.3
WHOI/URI	S, P, R, O, R	GU	24–42°N, 55°W	1980–85	39	SOFAR	700, 2000	563	60.1
WHOI	Owens/Price	SL	34°N, 70°W	1982–85	21	SOFAR	700	424	24.4
URI	Rossby	GF	Gulf Stream	1984–85	41	RAFOS	100–1700	34	3.8
WHOI	Price, Richardson	EB	32°N, 24°W	1984–88	32	SOFAR	1100	698	61.2
MAFF	Rees, Dickson	IB	Iberian Basin	1984–88	6	SOFAR	2500	918	15.1
IFREMER	Ollitrault	NO	N.E. Atlantic	1985–86	14	SOFAR	3800	262	10.1
MAFF/IOS	Rees, Gould	CB	Canary Basin	1985–88	7	SOFAR	3500	807	15.5
WHOI	Owens	NB	45°N, 40°W	1986–89	13	SOFAR	700, 1200, 2000	333	11.9
UW/URI	Rossby	SP	S.E. Pacific	1987–89	28	RAFOS	600–2600	220	16.9
URI	Rossby	AN	Gulf Stream	1988–89	20	RAFOS	100–1000	9	0.5
URI	Rossby	SY	Gulf Stream	1988–90	71	RAFOS	100–1300	31	6.0
Uiv. Tokyo	Taira	SB	N.W. Pacific	1988–91	9	SOFAR	1000–2000	371	9.1
WHOI	Richardson, Schmitz	TA	Tropical Atlantic	1989–92	41	SOFAR	800–3500	861	96.7
RSMAS	Leaman	AB	N.E. of Bahamas	1989–93	23	RAFOS	1000–3700	298	18.8
SIO	Davis	SA	South Atlantic	1990–93	8	ALACE	700	923	19.9
TOTAL				1972–93	498				451

NOTE: The Experiment Identifier is used by WHOI.
S, P, R, O, R = Schmitz, Price, Richardson, Owens and Rossby.

Table II: Summary of Proprietary Float Data Assembled by the WFDAC (November 1, 1995)

Institution	Source/PI	Experiment	Years	Location	# of Floats	Type	Nominal Depth (m)	Ave. Duration (days)	Total Float	Float Yrs	Availability
IFREMER	Ollitrault	TOPOGULF	1983–89	N. Atlantic	27	SOFAR	700	990	26732	73.2	1997
Univ. Kiel	Zenk, Boebel	Mediterranean	1990–94	Iberian B.	35	RAFOS	900	120	4193	11.5	1997
WHOI	Price, Owens	Subduction	1991–93	Canary B.	18	SOFAR	100–500	483	8688	23.8	Feb 1996
SIO	Davis	Pacific	1991–95	Pacific	~280	ALACE*	900	-	-	-	-
WHOI	Price, Richardson	Tracer Release	1992–93	Canary B.	10	SOFAR	200–600	173	1773	4.8	Feb 1996
Univ. Kiel	Zenk, Boebel	Deep Basin	1992–93	Brazil B.	10	RAFOS	800	137	1368	3.7	1997
SIO	Davis	Indian	1994–95	Indian	~175	ALACE*	800	-	-	-	-

*Most of the SIO ALACE floats are still operational.

Identifier	Experiment
MO	Mid Ocean Dynamics
RI	Gulf Stream Ring
PL	pre-LDE of Polymode
LD	LDE of Polymode
LR	Long-range test
GS	Gulf Stream test
GU	Gulf Stream recirculation
SL	Site L
GF	Gulf Stream
EB	Eastern Basin
IB	Iberian Basin
NO	NOAMP
CB	Canary Basin
NB	Newfoundland Basin
SP	South Eastern Pacific
AN	Anatomy
SY	Synop
SB	Shikoku Basin
TA	Tropical Atlantic
AB	Abaco
SA	South Atlantic Drake 90

Some recent float observations reflect work in the South Atlantic and Pacific Oceans.

The available float data can be obtained from NODC on the CD-ROM* or from WFDAC** on the Internet via Gopher software. A World Wide Web net server is being established; the home page will be linked to the Woods Hole Oceanographic Institution home page (http://www.whoi.edu). Along with the data set are (1) an index of floats giving basic information such as location, date,

* For more information or to purchase the CD-ROM contact: National Oceanographic Data Center, User Services Branch, NOAA/NESDIS E/OC21, 1825 Connecticut Ave., NW, Washington, DC 20235; Phone: 1-202-606-4549; Fax: 1-202-606-4586; Email: services@nodc.noaa.gov.

** P.L. Richardson, C.M. Wooding, Woods Hole Oceanographic Institution, Woods Hole, MA 02543-1541; Phone: 1-(508) 289-2546 PLR, 1-(508) 289-2722 CMW; Fax 1-(508) 457-2181; prichardson @whoi.edu, cwooding@whoi.edu.

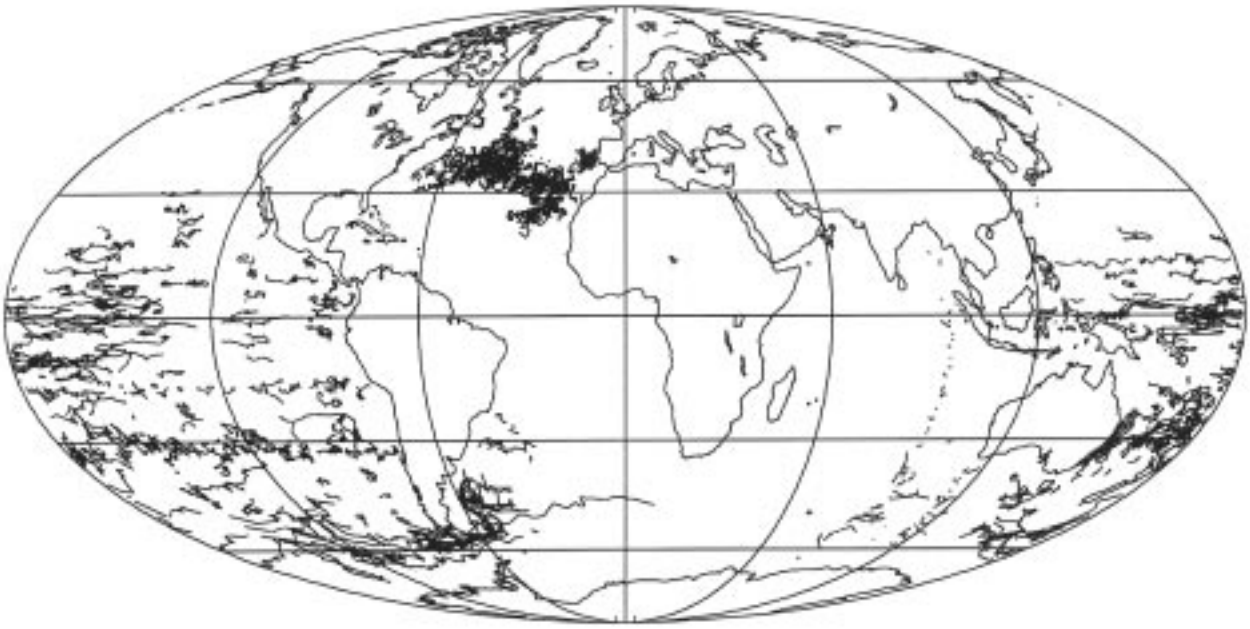

Figure 2. WOCE floats launched between 1990 and early 1995.

and depth, (2) summary plots and tables of trajectories in different regions, and (3) a list of data reports and scientific papers which describe the data and results of analyses. The data set and summary products are being updated at roughly yearly intervals, depending on data availability, and sent to NODC-WDCA.

In addition to the available float data are some data WFDAC has received which are still proprietary (Fig. 2, Table II). These include some additional historical SOFAR float data, some newer WOCE SOFAR, ALACE and RAFOS data in the North Atlantic, some RAFOS and ALACE data in the South Atlantic, and some ALACE data in the Pacific and Indian Oceans. WFDAC receives yearly updates of the WOCE ALACE data. To obtain or use any of these data please contact the source or P.I. listed in Table II.

Approximately 1200 floats have been launched since 1990, most of them as part of WOCE. The new WOCE float data have just started to be assembled by the WFDAC. Many WOCE floats are still drifting or being tracked and many others have not yet been launched. For example we have only received a handful of the trajectories from the South Atlantic where approximately 400 RAFOS-type floats have been or will be launched. Roughly 100 RAFOS floats in the North Atlantic are still being tracked. The 280 Pacific ALACE floats are starting to yield a significant data set but most of them are still drifting. The 100 North Pacific RAFOS are surfacing in 1995 and are being tracked. Roughly 175 ALACE floats were launched in the Indian Ocean, but they have just begun their 5-year mission which explains the short trajectories in Fig. 2. Approximately 600 floats are planned to be launched as part of the Atlantic Climate Change Experiment and other experiments which will take place in the North Atlantic during 1996–1997. Some floats will continue to drift to year 2000. A detailed list of expected float data has been prepared by the WOCE Data Information Unit and can be seen on the World Wide Web http://www.cms.udel.edu (called OCEANIC).

Although we have already assembled a fairly large amount of float data as seen in Figs. 1 and 2, the data set which will be available by the end of the century will be many times larger. We are only seeing the tip of the WOCE float iceberg in Fig. 2. By year 2000 a map like the ones in Figs. 1 and 2 would show the oceans almost completely filled with thermocline floats and a few deeper floats primarily in the Atlantic and northwestern Pacific. To help interested scientists learn about the available float data as they are assembled during the next several years, WFDAC will periodically update the summary plots and tables.

The WFDAC is funded by the National Oceanographic and Atmospheric Administration Climate and Atmospheric Research Program, Grant Numbers NA46GPO133 and NA56GPO260 to the Woods Hole Oceanographic Institution.

WHPO Status Reports

The WOCE Hydrographic Programme Office (WHPO) publishes status reports 2–3 times per year. These reports describe the activities of the office which include WOCE cruise plans and cruise reports received, data reports produced, and WHP datasets transferred to the SAC (and thus in the public domain). To keep abreast of the field work WOCE participants are encouraged to view these documents periodically. They can be found on the WWW at:

http://www.whoi.edu/status.html

Control of the Deep Circulation in the Brazil Basin by the Sill in the Romanche Fracture Zone

Harry Bryden, Southampton Oceanography Centre, Southampton, SO14 3ZH, UK, and Herlé Mercier, Laboratoire de Physique des Océans, IFREMER, 29280 Plouzané, France

Introduction

In the hydrographic section along the axis of the Romanche Fracture Zone (Fig. 1) presented by Speer, Mercier, Messias and Mémery (1994), it appears that the Antarctic Bottom Water (AABW) has filled up the reservoir behind the sill: the deep water with potential temperatures below 0.8°C is fairly uniform while there is a sharp benthic thermocline between 1°C and 2°C above the reservoir. In fact, Speer *et al*. (1994) noted that a sill depth control appeared to be exerted near 1°C. The impression is that, as the reservoir filled, the deep water has pushed the warmer isotherms upward, compressing the vertical stratification above the reservoir until the AABW can somehow escape over the sill. It does not appear from the section, however, that there is any direct ventilation of the AABW reservoir below 0.8°C.

Model

For a steady state situation where there is a source of AABW, U, entering the reservoir from the west (and eventually from the south), the upward flow, w, across isotherms which are effectively blocked by the sill implies that the reservoir is gaining heat, presumably by diffusion from above down through the benthic thermocline:

$$U_R\theta_R + \int w\theta(z)dx = \int k\frac{\partial\theta(z)}{\partial z}, \qquad (1)$$

where U_R is the source of AABW with potential temperature θ_R, $\theta(z)$ represents the vertical structure in potential temperature, k is the turbulent vertical (cross-isothermal) diffusion coefficient, and x is the along-section coordinate. By mass conservation, of course, $U + \int wdx = 0$, so the heat balance (1) can be rewritten as:

$$\int dx\left(w\left(\theta(z) - \theta_R\right) = k\frac{\partial\theta(z)}{\partial z}\right). \qquad (2)$$

Thus, for uniform vertical velocity and constant diffusion coefficient and for depths below the effective sill depth, there should be a linear relationship between potential temperature and vertical potential temperature gradient:

$$\frac{\partial\theta(z)}{\partial z} = \frac{w}{k}\left(\theta(z) - \theta_R\right). \qquad (3)$$

The process leading to this relationship is that as the reservoir fills it compresses the isotherms above the reservoir until sufficient heat can diffuse downward through the resulting benthic thermocline to warm the top of the reservoir enough to allow an amount of water equal to the reservoir source strength to escape over the sill.

To test this relationship, we plot the average vertical potential temperature gradient for stations 4, 9 and 10 in the upstream reservoir (Mercier *et al.*, 1992) against potential temperature (Fig. 2). There does appear to be a nearly linear relation for potential temperatures below 1.4°C and we estimate the intercept, θ_R, to be 0.8°C and the slope, w/k, to be 0.86 x 10^{-4} cm^{-1}. We interpret the break in the linear relationship at 1.4°C, or about 4200 m depth, to represent the depth above which there is relatively free passage for the AABW out of the reservoir into the eastern Atlantic.

We previously estimated on the basis of hydraulics arguments (Mercier and Bryden, 1994) that 2.4 Sv of AABW was flowing across the sill of the Romanche Fracture Zone. To determine the appropriate vertical velocity then, it is necessary to decide how large the area is over which the vertical transfer occurs. Is it just the relatively small area of the Romanche Fracture Zone? Or is it the area of the entire Brazil Basin as far south as its southern entrance at Vema Channel? Examining 4 zonal hydrographic sections across the Brazil Basin presented by McCartney (1993) and McCartney and Curry (1993), we find little evidence for a benthic thermocline at 23°S; a benthic thermocline in the interior at 16°S away from western boundary influences; at 11°S the evidence is clouded by a nonuniform choice of isotherm contours; and at 8°S there is a clear benthic thermocline across virtually the entire Brazil Basin. Thus, it appears that over about half of the Brazil Basin, an area of approximately 3 x 10^6 km^2, the AABW reservoir has pushed the deep isotherms upwards to create a benthic thermocline. Distributing the 2.4 Sv of AABW flow across the Romanche sill over this reservoir area then yields an average vertical velocity of w = 0.8 x 10^{-4} cm s^{-1} and a vertical diffusion coefficient of k = 0.9 cm^2s^{-1}. Such a vertical velocity is very close to the estimate by Speer and Zenk (1993) for w across σ_4 = 45.85 in the Brazil Basin based on the convergence of meridional Bottom Water transports across 30°S and 11°S.

Discussion

Hogg *et al.* (1982) made similar, more careful estimates of w and k for the entire Brazil Basin by examining the thermal structure of the AABW flowing into Brazil Basin at its southern entrance through the Vema Channel and outflowing over the Ceara Rise at the northern exit and by analysing the average vertical temperature gradient throughout the Brazil Basin at the 1.6°C, 0.8°C and 0.0°C isotherms. Clearly, one of the primary issues for analysis of the Deep Basin Experiment is to do that analysis again

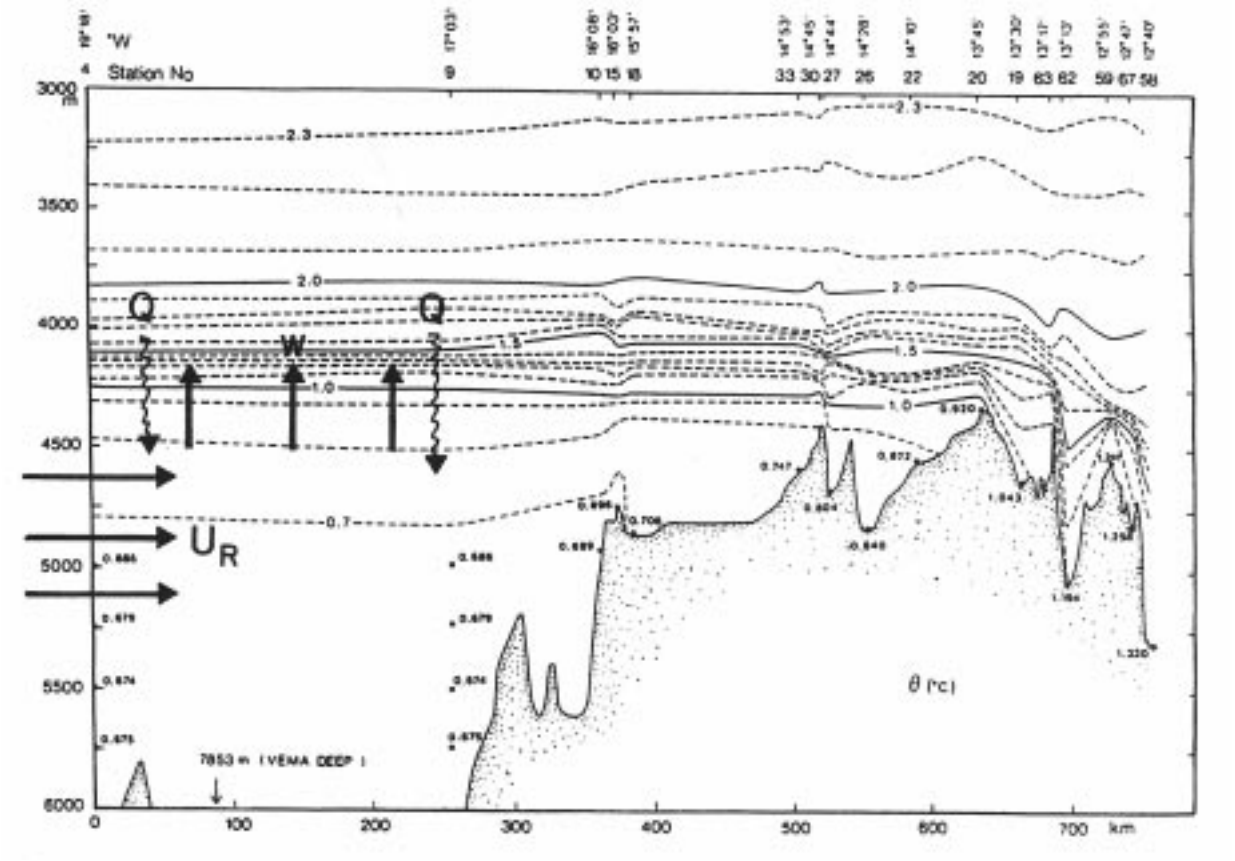

Figure 1. Potential temperature (°C) below 3000 m depth along the axis of the Romanche Fracture Zone. Bottom profile represents the deepest point of the fracture; the walls on either side are typically 3000–3500 m deep, so the section is mostly within the fracture zone. This is Fig. 2 of Speer, Mercier, Messias and Mémery (1994). Added are arrows denoting the source of Antarctic Bottom Water (AABW), U, for the deep reservoir, vertical velocities across isotherms below sill depth, and squiggly arrows representing downward diffusion of heat, $Q = -k\frac{\partial\theta}{\partial z}$*, through the benthic thermocline.*

with all of the inflows and outflows carefully measured (Hogg, 1994). Here, with the simpler estimates presented above, we choose to emphasise the control exerted by the Romanche sill on the structure of the upstream reservoir of AABW, in particular on generating the benthic thermocline in the Brazil Basin.

Hogg *et al.*'s estimates for k were 3 to 4 cm^2s^{-1}, a factor of 4 to 5 larger than our estimates above. This disparity is partially due to Hogg *et al.*'s use of the larger source of AABW of 4.1 Sv through Vema Channel in contrast to our emphasis on the smaller amount of AABW exiting over the Romanche sill. Our view of the flow of AABW through the Brazil Basin is that much of it takes place in a northward flowing western boundary current along the South American continental slope which eventually passes out of the Basin in the region of the Ceara Rise at about 4°N, 40°W. This flow warms by mixing as it travels through the Basin in what are referred to as boundary mixing processes. Our estimate for k, in contrast, is for interior vertical (cross-isotherm) mixing away from the boundaries that heats up the deep interior reservoir so it can escape out of the Basin. Hogg *et al.*'s estimates for k represented averages over the entire Brazil Basin and hence combine interior and boundary mixing processes. As Hogg (1994) notes, separating boundary mixing from interior mixing is a key issue for the Deep Basin Experiment.

Now it is possible that the flow over the Romanche sill above 1°C is fed directly at least in part by the western boundary current turning eastward along the equator. In such a situation, the estimate of interior mixing above would need to be reduced. The estimate of $k = 0.9\ cm^2\ s^{-1}$ then is perhaps an upper bound on the amount of interior mixing.

Our interpretation of the break in slope between temperature gradient and temperature at a potential temperature of about 1.4°C (Fig. 2) is that there is relatively free exit of water warmer than 1.4°C out of the Brazil Basin over the eastern and western sills. The section along the Romanche Fracture Zone clearly shows that 1.4°C water passes over the sill and cascades down into the eastern Atlantic. In the western sill region, McCartney's (1994) analysis suggests that the sill depth is about 4200 to 4250 m there, that 1.4°C water does pass over the sill, and that the bathymetry resembles a channel with a small sill obstruction rather than the towering dam evident in the Romance Fracture Zone. Thus, for either the eastern or western exits,

there appears to be relatively free flow of water warmer than 1.4°C out of the Brazil Basin and hence the Romanche sill no longer directly controls the thermal stratification above 1.4°C.

Recent estimates of the transports of AABW out of the Brazil Basin are 2.4 Sv over the Romanche sill (Mercier and Bryden, 1994) and 2.1 Sv in the western equatorial region (Hall, Whitehead and McCartney, 1994). If these values are right, one might ask why one finds water with stronger AABW characteristics in the western North Atlantic than in the eastern tropical Atlantic south of the Vema Fracture Zone at 11°N. Our answer would be to point out the differing nature of the two exit flows. The exit flow in the west appears to follow the relatively gentle slopes of the South American continental slope and mid Atlantic Ridge, slowly descending and mixing. In contrast, the exit flow over the Romanche sill appears to cascade downward over the sill, violently mixing as it descends (Polzin, Speer, Toole and Schmitt, 1995). In the arguments of Price and Baringer (1994), the steeper slope at the Romanche sill causes mixing and entrainment downstream of the sill that extinguish the signature of AABW in the eastern Atlantic. The slopes in the western exit region are presumably not large enough to cause such violent entrainment so that the AABW signature is stronger in the western North Atlantic.

Finally, the interior upward vertical velocity at the top of the AABW reservoir implies a clockwise circulation of the AABW reservoir in an argument based on Stommel and Arons (1960) theory:

$$\int v dz = \frac{f}{\beta} w, \qquad (4)$$

where v is northward velocity, f is the Coriolis parameter and β is its northward derivative and z is the vertical coordinate. Choosing f and β for a latitude of 10°S in the mid Brazil Basin and using $w = 0.8 \times 10^{-4}$ cm s^{-1} as determined above yields a southward interior transport of 1.5 Sv over the 15° longitude width of the Brazil Basin, which is presumably balanced by a supplemental northward flow in the western boundary current of 1.5 Sv added to the AABW throughflow. Speer and Zenk (1993) did present evidence for southward flow of Bottom Water in the interior of the Brazil Basin across 24°S and 11°S, though the magnitude of their southward transports appear to be of order 5 Sv. In an inverse argument, measuring the western boundary current transport of AABW above the amount of throughflow could allow an independent estimate of the interior upwelling and mixing.

Conclusion

In summary, we identify the sill at the eastern end of the Romanche Fracture Zone as the control for much of the deep circulation of the Brazil Basin. This sill, apparently the deepest exit sill for the Basin, blocks the reservoir of AABW behind it leading to the creation of a benthic

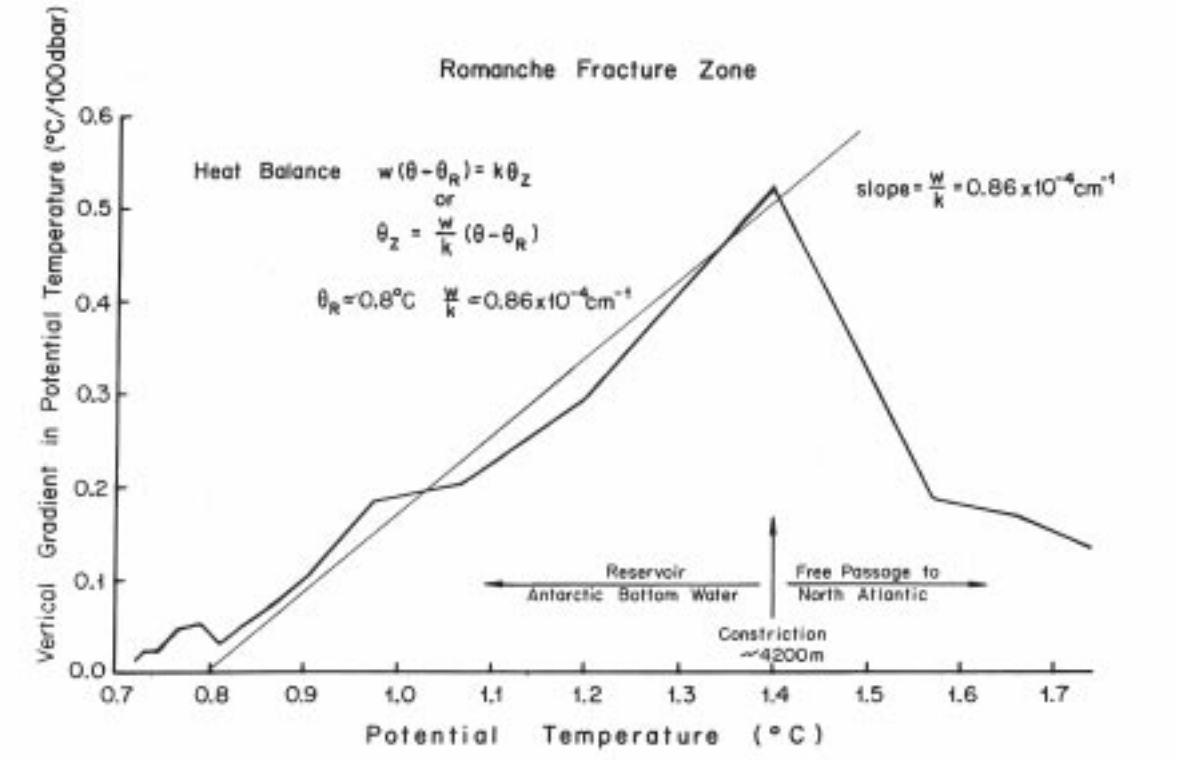

Figure 2. Vertical gradient of potential temperature plotted against potential temperature for stations 4, 9 and 10 in the upstream reservoir behind the Romanche sill in Fig. 1. The line is an estimate of the relationship between potential temperature gradient and temperature between 0.8°C and 1.4°C. Above 1.4°C, which is at a depth of about 4200 m, there is relatively free passage for water to leave the Brazil Basin and enter the eastern Atlantic.

thermocline between 0.8°C and 1.4°C over most of the interior Brazil Basin. The resulting vertical velocity drives a clockwise circulation of the AABW reservoir which must supplement the throughflow of AABW along the western boundary. Clearly, more careful and refined calculations must be carried out once all of the Deep Basin Experiment measurements are completed. Yet it is hard to escape the conclusion that the sill in the Romanche Fracture Zone plays a crucial role in determining the circulation of the Brazil Basin.

References

Hall, M.M., J.A. Whitehead, and M.S. McCartney, 1994: Moored measurements of Antarctic Bottom Water at the equator. International WOCE Newsletter, 17, 5–8.

Hogg, N., 1994: Status of the Deep Basin Experiment. International WOCE Newsletter, 17, 3–4.

Hogg, N., P. Biscaye, W. Gardner and W.J. Schmitz, Jr., 1982: On the transport and modification of Antarctic Bottom Water in the Vema Channel. J. Mar. Res., 40 (Supplement), 231–263.

McCartney, M.S., 1994: The transport of Antarctic Bottom Water at 4°N in the western basin of the North Atlantic Ocean. J. Geophys. Res., accepted.

McCartney, M.S. and R. A. Curry, 1993: Transequatorial flow of Antarctic Bottom Water in the western Atlantic Ocean: Abyssal geostrophy at the equator. J. Phys. Oceanogr., 23 (6), 1264–1276.

Mercier, H., A. Billant, P. Branellec, P. Morin, M.-J. Messias, L. Mémery, C. Thomas, and J. Honnorez, 1992: Campagne Romanche 1, l'Atalante (10 août-8 septembre 1991), Données $CTDO_2$, Chimie et Bathymétrie. Laboratoire de Physique des Océans, Unité mixte de Recherche no. 127, Rapport Interne LPO 92-02.

Mercier, H., and H. Bryden, 1994: Flow of Antarctic Bottom Water over the sill in the Romanche Fracture Zone. International WOCE Newsletter, 17, 9–10.

Polzin, K., K. Speer, J. Toole and R. Schmitt, 1995: Intense mixing of Antarctic Bottom Water in the equatorial Atlantic. International WOCE Newsletter, 19, 20–23.

Price, J.F., and M.O'N. Baringer, 1994: Outflows and deep water production by marginal seas. Progress In Oceanography, 33, 161–200.

Speer, K., H. Mercier, M.-J. Messias and L. Mémery, 1994: The Romanche Fracture Zone: Blocking and mixing of Arctic and Antarctic waters at the equator. International WOCE Newsletter, 16, 8–11.

Speer, K.G., and W. Zenk, 1993: The flow of Antarctic Bottom Water into the Brazil Basin. J. Phys. Oceanogr 23, 2667–2682.

Stommel, H., and A. Arons, 1960: On the abyssal circulatin of the world ocean-I. Stationary planetary flow patterns on a sphere. Deep-Sea Res. 6, 140-154.

The Problem of Meridional Heat Transport in the Pacific Sector of the Antarctic

M.N. Koshlyakov and T.G. Sazhina, P.P.Shirshov Institute of Oceanology, Russian Academy of Sciences, Moscow, 117851, Russia

In a previous paper (Koshlyakov and Sazhina, 1995, later KS) we have estimated the meridional heat transport, connected with the baroclinic component of large-scale geostrophic current, across the section S4 Pacific (S4P), using the CTD data of this section. The baroclinic component of the current at every station was determined as the difference between the total geostrophic current and its average over the full depth. Now in this paper we develop this approach to the heat transport problem, dividing the baroclinic current into its average along the section and the deviation from this average. Following Saunders and Thompson (1993), we can write for every ocean level:

$$\int V(bc)\theta dx = V(mbc)\theta(m)L + \int V(dbc)\theta(d)dx \quad (1)$$

Here the integration is carried out over the whole section length. V(bc) is a component of the baroclinic velocity normal to the section; θ is a potential temperature; L is a section length at the given level; letters m and d denote correspondingly the average over the section length and deviation from it.

The term V(mbc) θ(m) L determines the heat transport connected with the vertical water circulation (overturning effect) in the area between S4 and the Antarctic Continent (see Fig. 1 in KS). Fig. 1 shows the vertical densities of the heat transport across the S4P connected with the first and second terms in the right side of (1). Lines 1 and 2 of Table 1 represent the integral of this vertical distribution over the full depth; line 3 represents the similar integral of the vertical density of the total baroclinic heat transport. The product V(mbc) θ(m) changes its sign at the level 2000 m (upper curve in Fig. 1), that is connected with the change of the direction of V(mbc) at the same level (see Fig. 4 in KS). This product tends to zero in the layer below 3400 m because θ(m) approaches zero there (Fig. 2 in KS). According to Table 1, the southward integral of heat transport across S4P, directly connected with the vertical circulation in the Antarctic area to the south of this section is equal to 0.038 pW, or 1.2 10^{21} J yr^{-1}. It looks like a reasonable value because the annual heat flux from the ocean to the atmosphere in the entire ocean area southward the Southern Polar Front is about 1.0 10^{22} J yr^{-1}. (Gordon, 1988), and the square of the area between this Front and the Antarctic Slope is one order more than the square of the area between the S4P and this slope ($35 \cdot 10^6$ and $2.7 \cdot 10^6$ km^2, correspondingly).

It should be emphasized that the replacement of V(bc) by the total geostrophic current velocity (baroclinic plus

Table 1. Heat transport (pW) across the section S4P. The sign minus corresponds to the transport into the Antarctic area.

By baroclinic current, averaged along the section	-0.0378
By deviation of baroclinic current from the average along the section	0.0054
By total baroclinic current	-0.0324
By total (barotropic plus baroclinic) current averaged along the section	-0.0374

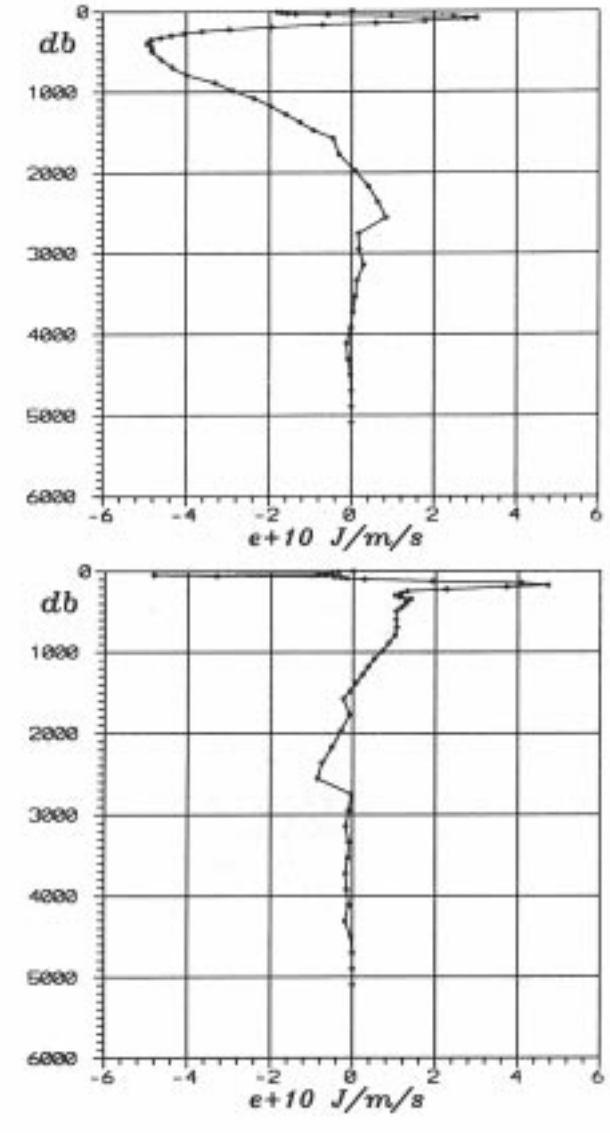

Figure 1. Vertical density (in 10^{10} J m^{-1} s^{-1} of the heat transport across the entire S4P section, induced by the baroclinic current averaged along the section (above) and by the deviation of baroclinic current from this average (below). Negative values correspond to heat transport (referred to temperature in °C) into the Antarctic area.

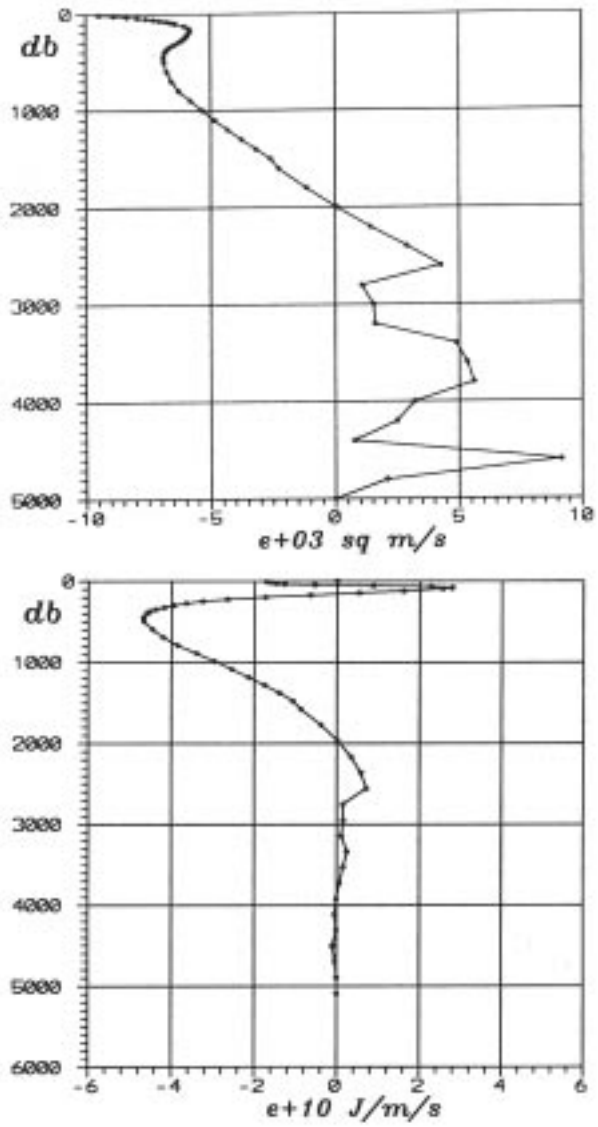

Figure 2. Above: vertical density (in 10^3 m^2 s^{-1}) of the volume transport of total geostrophic current across the entire S4P section; negative values correspond to the current into the Antarctic area. Below: vertical density (in 10^{10} J m^{-1} s^{-1}) of the heat transport across the entire S4P section, induced by the total geostrophic current averaged along the section; negative values correspond to heat transport (referred to temperature in °C) into the Antarctic area.

barotropic) cannot considerably change the upper curve in Fig. 1 and the quantity in the first line of Table 1, because the averaging along the coast-to-coast section strongly eliminates the barotropic current (eliminates completely in a case of constant ocean depth). This statement is supported by the curves in Fig. 2 and the quantity in the fourth line of Table 1, which were calculated using the estimation of the total geostrophic current across the S4P (see KS). The upper curve in Fig. 2 and the similar curve for the baroclinic current (Fig. 4 in KS) look rather different from each other below 3000 m because of the bottom relief. At the same time the volume of southward and northward transports are

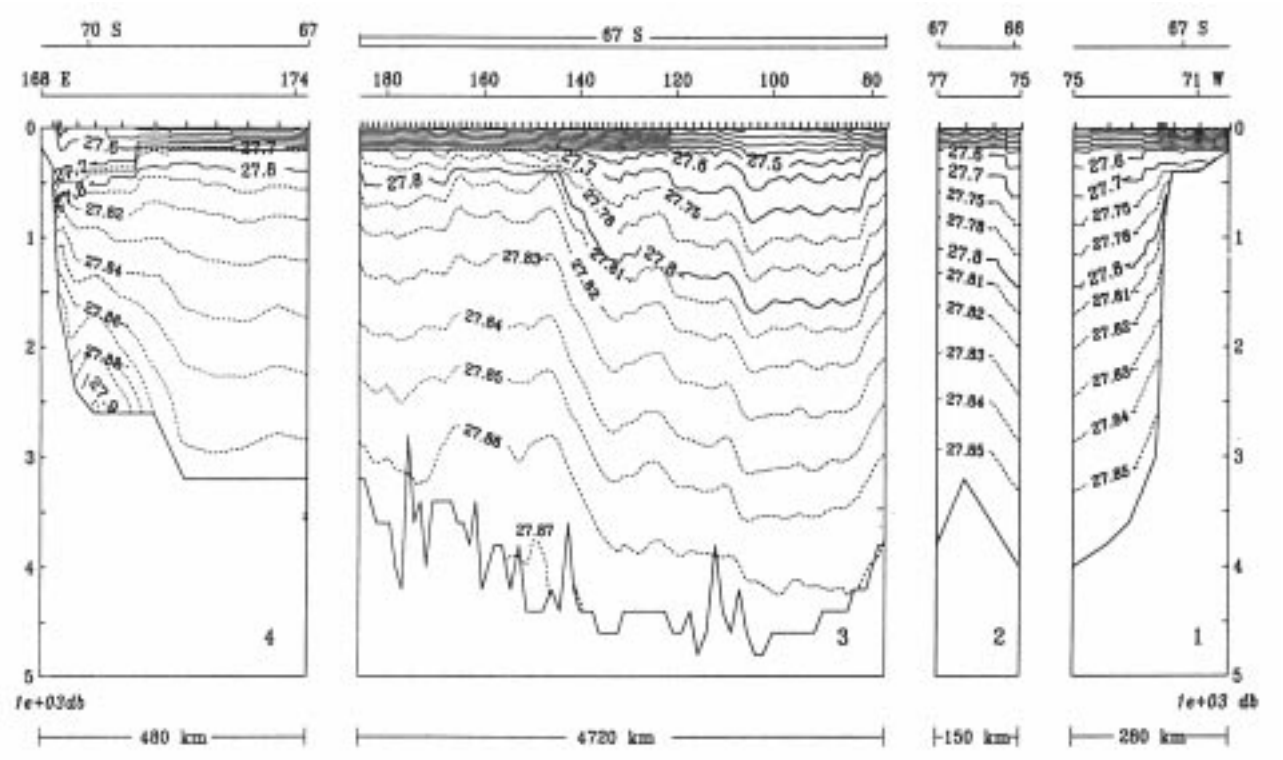

Figure 3. Potential density $\sigma(S,\theta,0)$(kg m^{-3}) in the section S4P from the Antarctic Peninsula (70°W) to the Pennell Coast (168°E). Horizontal scale for part 3 of the section is five times less than that for parts 1, 2 and 4. The marks on the ocean surface line indicate CTD stations.

identical (7.9 Sv) for these two curves. The upper curve in Fig. 1 and the lower curve in Fig. 2, as well as the quantities in the first and the fourth lines of the Table 1, are also practically identical, due to closeness to zero and small vertical gradient of the potential temperature in the deep layer (Fig. 2 in KS). That is an important result showing that the characteristics of heat transport, connected with the vertical circulation and presented in Figs. 1 and 2 and in Table 1, practically does not depend on the barotropic current and, consequently, on the errors of determination of this current (see KS). Fig. 3 shows that within the range 27.81 – 27.86 all the intersections of these isopycnals with the Continental Slope at the western edge of the S4P are located much shallower than the corresponding points at the eastern flank of the section. This circumstance is the direct cause of the vertical circulation existence, demonstrated by Fig. 2 of this paper and Fig. 4 in KS. As it can be seen from Fig. 3, only 15% of this global slope of isopycnals could be explained by the process of autumn convection starting in the end of March at the very western flank of the S4P and resulting in the local rise of isopycnals 27.83 to 27.87 just near the Continental Slope. So we can suppose that our conclusion about the presence of a mean overturning circulation in the Pacific Sector of the Antarctic has climatological sense. Naturally, this work cannot give any direct answer to the question, in what part of this big sector the overturning process is mainly located. It is very possible that the Ross Sea could be such a region because of the generation of the Antarctic Bottom Water in this sea (see Fig. 3 in KS and the spot of very dense water near the bottom at the western flank of the S4P in Fig. 3 of this paper).

Acknowledgements

This work is supported by grant N 94-05-16179-a of the Russian Foundation for Fundamental Research and by grant N NDX000 of the International Science Foundation.

References

Gordon, A.G., 1988: Spatial and temporal variability within the Southern Ocean. In: Antarctic Ocean and Resources Variability (ed. D.Sahrhage). Springer-Verlag, Berlin, 41–56.

Koshlyakov, M.N., and T.G. Sazhina, 1995: Meridional volume and heat transport in the Pacific Sector of the Antarctic. In: International WOCE Newsletter, Number 18, 3–6.

Saunders, P.M., and S.R.Thompson, 1993: Transport, heat and freshwater fluxes with a diagnostic numerical model (FRAM). J. Phys. Oceanogr., 23(3), 452–464.

Is the Deep Water Circulation in the Argentine Basin Going Round the "Wrong" Way?

Denise Smythe-Wright and Stephen Boswell, Southampton Oceanography Centre, Empress Dock, Southampton, SO14 3ZH, UK

The abyssal water mass in the Argentine Basin, the Antarctic Bottom Water (AABW), is of southern origin. Its source is primarily Weddell Sea Deep Water (with characteristics of -0.7 – +0.2°C and salinity 34.65 – 35.68), which flows out of the Weddell gyre into the South Sandwich trench and continues north through the Falklands Escarpment into the Basin. It cannot have a source in the Antarctic Circumpolar Current (ACC) since waters colder than 0.2°C are not associated with the ACC in the Drake Passage. A description of the inflow of AABW into the Argentine Basin has been given by Whitworth *et al.*, 1991. Once it has entered the Argentine Basin from the South Georgia Basin, through gaps in the Falklands Escarpment, it is assumed that it turns left, following the theory of Stommel and Arons (1960). It continues along the continental shelf as a western boundary current which flows under the Brazil-Falklands confluence region and up the coast of Argentina to enter the Brazil Basin west of the Rio Grande Rise. Results from the WOCE A11 section (Fig. 1), occupied December 1992–February 1993 from RRS Discovery, would, however, suggest that its northward passage through the Argentine Basin is not simply controlled by classical oceanographic theory.

At first sight it would appear from the temperature and salinity profiles (Fig. 2) that the Bottom Water in the Argentine Basin is fairly uniform. But traditional measurements cannot distinguish between dense water that has recently entered the Basin and water which has been in residence for some time. The CFC profile across the Basin (Fig. 3), however, suggests, that the newest, most CFC-rich water, is found on the eastern flank. If a predominant western boundary flow was correct, then the CFC data should show highest concentrations on the western side of the basin. The CFC section at 45°S shows this is clearly not the case.

Recent evidence from ADCP measurements (Saunders and King, 1995), mud waves (Flood and Shor, 1988), and current meter moorings (Weatherly, 1993; Whitworth *et al.*, 1991) suggest that there is an anticlockwise circulation around the Zapiola Drift. Closer inspection of the CFC data agrees with this. From the CFC-11:CFC-12 ratio it appears that the water on the eastern side of the Zapiola Drift is 2 years younger than on the western side. However, the temperature and salinity characteristics reveal that the water west of the Zapiola Drift is, at any given depth below 4000 m, warmer and saltier than to the east. This implies entrainment of overlying Circumpolar/Brazil Confluence water. Simple mixing estimates suggest that there is up to 30% dilution by the overlying water and on this basis the "age" difference between the western and eastern water is reduced to 1 year. Assuming a rough trajectory of 2300 km from east to west then this results in a transportation rate of 7 cm s^{-1} which agrees well with other estimates of the anticyclonic flow in the Basin.

Since the CFC "high" extends across the eastern Argentine Basin and appears to follow two distinct plumes, we suggest that the abyssal water enters the basin from the South Georgia Basin, predominantly at a gap in the Falkland Escarpment at 36°W (Whitworth *et al.*, 1991) and to the east of the Islas Orcadas Rise at about 28°W. Rather than turning west, a large proportion flows north to north-eastwards and continues east of the Zapiola Drift, possibly

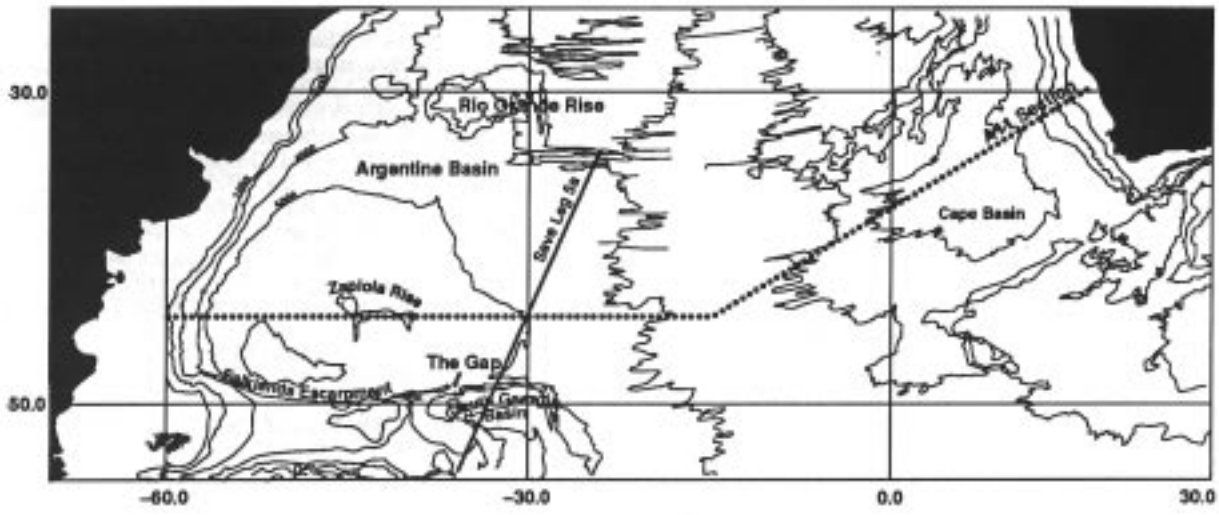

Figure 1. The All section, notionally along 45°S from the Argentine coast to the mid ocean ridge and then northeast to the African coast at 30°S.

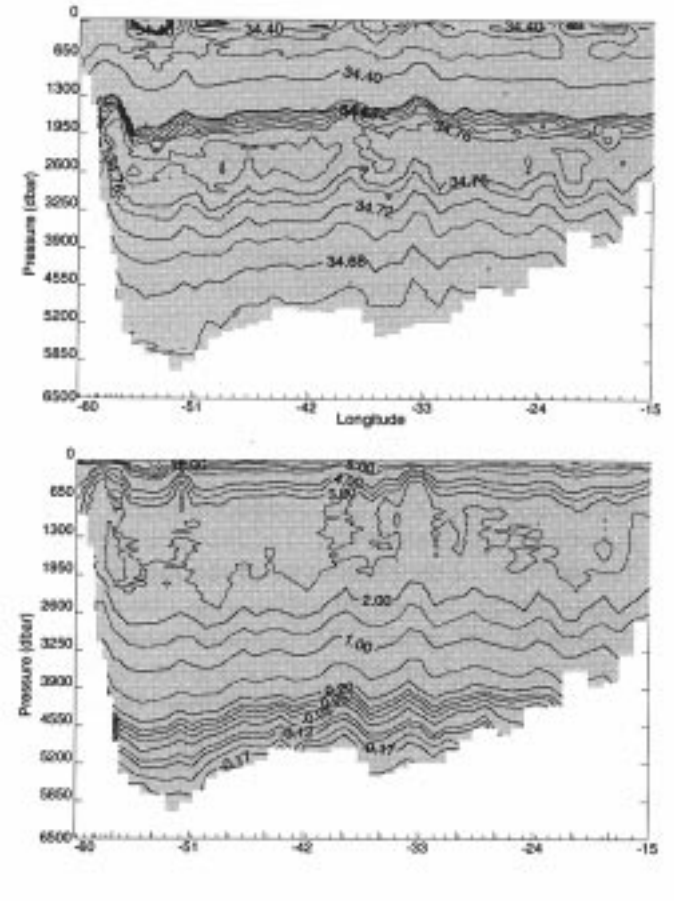

Figure 2. Temperature and salinity across the Argentine Basin at 45°S.

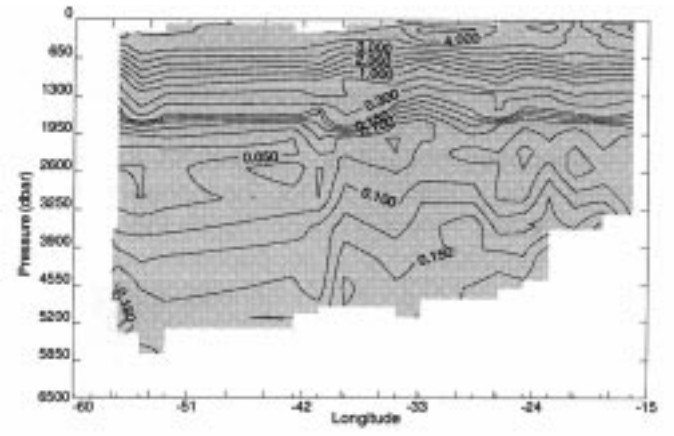

Figure 3. CFC-11 section along 45°S in the Argentine Basin.

spreading north to the Brazil Basin. This conclusion is supported by data from two meridional sections, at 27°W (SAVE Leg 5) and along 25°W (Tsuchiya *et al*., 1994), which show that the signature of the Weddell Sea sourced water extends to at least 40°S.

It must be stressed that the CFC data do not rule out the existence of the western boundary current. CFC "highs" are seen on the western flank of the Argentine Basin which support such a northward movement of AABW. Here the concentrations are slightly lower than on the eastern side but allowing for a small dilution from overlying water (about 10%) they reflect about a 9 month time difference in the age of eastern and western waters. Since the western water will have travelled approximately 1400 km further (along the northern side of the Falklands Escarpment) to reach 45°S than its eastern counterpart which just moves due north, such a time difference is not unrealistic. It suggests an average translation rate of 6 cm s^{-1} which is consistent with the current meter data of Whitworth *et al*., 1991. It therefore seems reasonable to suggest that the flow of abyssal water bifurcates once it reaches the northern side of the Escarpment, with the most dominant branch moving north northeast to form an anticyclonic flow around the Zapiola Drift.

The reason for the anticyclonic flow is unclear, but it is likely that it is related to the meandering pattern of the circumpolar fronts which delineate the ACC. The influence of the fronts and transport of the ACC is known to extend to bottom depths (Tsuchiya *et al.*, 1994). There is evidence of spatial coincidence of two of the fronts of the ACC in this region (Peterson and Whitworth, 1989). When this occurs the ACC appears as a single front slightly further south of its mean position of 48.5°S. As a consequence the western flow of water along the Falklands Escarpment is squashed and becomes less intense. The results of Whitworth *et al*., 1994 show that there is a persistent meander in the ACC slightly west of the gap in the Falklands Escarpment at 36°S and from a 14 month current meter record they observed changes in the intensity of the eastward and westward flows associated with a north-south movement of this meander. We therefore conclude that it is the migratory nature of the ACC which reduces the western boundary flow, and, in turn, it is the ACC's intense easterly movement which constrains the flow of the Bottom Water so that it follows a north northeasterly direction. Once north of 40°S the effect of the ACC reduces and flow turns west to form the anticyclonic flow around the Zapiola Drift.

References

Flood, R.D., and A.N. Shor, 1988: Mud waves in the Argentine Basin and their relationship to regional bottom circulation patterns. Deep-Sea Res., 35, 943–971.

Peterson, R.G., and T Whitworth (III), 1989: The Subantarctic and Polar fronts in relation to deep water masses through the southwestern Atlantic. J. Geophys. Res., 94, 10817–10838.

Saunders, P.M., and B.A. King, 1995: Bottom currents derived from a shipborne ADCP on WOCE Cruise A11 in the South Atlantic. J. Phys. Oceanogr. 25, 329–347.

Stommel, H., and A.B. Arons, 1960: On the abyssal circulation of the world ocean; An idealised model of the circulation pattern and amplitude in oceanic basins. Deep-Sea Res., 6, 217–233.

Tsuchiya, M., L.D. Talley and M.S. McCartney, 1994: Water mass distributions in the western South Atlantic; A section from South Georgia Island (54°S) northward across the equator. J. Mar. Res., 52,55-81.

Weatherly, G., 1993: On deep-current and hydrographic observations from a mudwave region and elsewhere in the Argentine Basin. Deep-Sea Res., 40, 939–961.

Whitworth, T., (III), W.D. Nowlin, Jr., R.D. Pillsbury, M.I. Moore and R.F. Weiss, 1991: Observations of the Antarctic Circumpolar Current and Deep Boundary Current in the Southwest Atlantic. J. Geophys. Res., 96, 15105–15118.

Preliminary Results From a WHP Section in the Central Indian Ocean

Lynne D. Talley, Scripps Institution of Oceanography, La Jolla, CA 92093-0230, USA, and Molly Baringer, NOAA/AOML, 4301 Rickenbacker Causeway, Miami, FL 33149

Work carried out along WOCE section I8N/I5E occupied on RV Knorr (10 March 1995 to 15 April 1995), was described briefly in Talley (1995). The section crossed the centre of the Central Indian Basin and repeated the 1987 crossing of northward deep water flow west of Australia (Toole and Warren, 1993). A small source of Central Indian Basin deep water was surveyed. The cruise track, Columbo south along 80°E (I8N) then east along 32°S (I5E), was shown in the September issue of the newsletter; updated versions are available through netscape or ftp (ftp://nemo.ucsd.edu/woce/plots, click on woceind_label.gif). A cruise report and vertical sections are available from Talley (ltalley@ucsd.edu) and a condensed version of this note with additional figures can be found at http://www.aoml.noaa.gov/general/project/phodmob4.html.

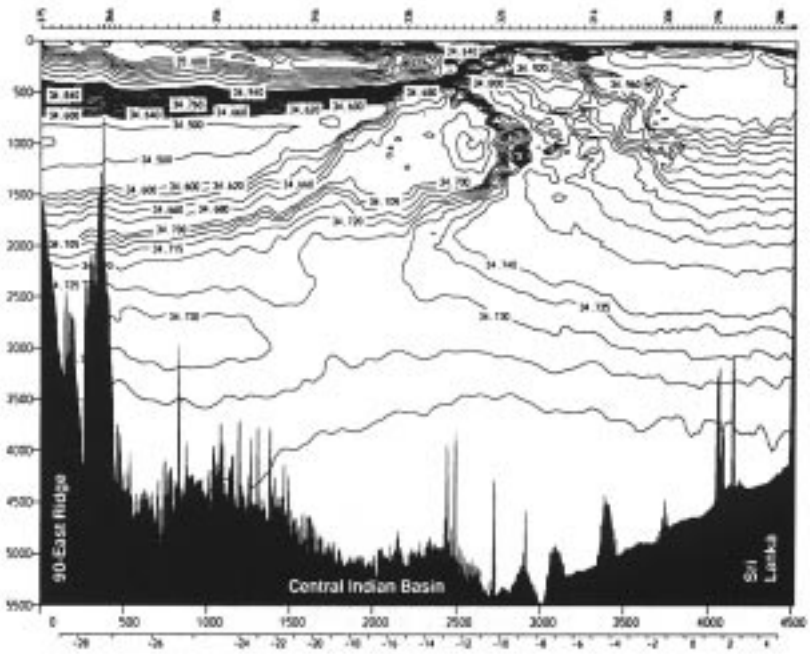

Figure 1a. Salinity along I8N at 80°E.

Potential temperature was shown in the previous issue (Talley, 1995); salinity along the 80°E and 82°S sections (Figs. 1a and b) is a good basis for description of the basic features. Velocity/transport estimates listed below are preliminary as no attempt has been made to balance mass. Unless otherwise stated, a reference level of zero velocity at the bottom is used.

Surface and intermediate water masses and geostrophic currents

Fresh surface water (<33.3 off Sri Lanka and <34.2 at 5°S) extends southward from Sri Lanka to a front at 10°S and originates in the north-eastern Indian Ocean. Below the fresh surface water lies an intense halocline centred mostly around 60 m depth with approximately a 1.1 psu change over 10 m. The saline water (>35.3) just below the halocline is of Arabian Sea origin. The halocline is deepest off the Sri Lankan coast, where there appears a narrow westward coastal jet in the surface layer (>40 cm s^{-1}), and a narrow eastward jet in the saline layer below down to 400 m (>10 cm s^{-1}); the eastward flow appears to extend as deep as 2200 m. Westward transport in the surface jet may be 6 Sv; eastward transport below is about 30 Sv.

Temperature/salinity/density indicate an equatorial undercurrent centred at about 80 m on this March section, in accord with climatology (Knox and Anderson, 1985). The westward surface current has velocities of about 70 cm s^{-1}. The equatorial currents are confined between fronts at 4°N and 4°S, and the low salinity surface water is higher than north and south of this equatorial channel; the halocline is also more intense at the equator. Brunt-Väisälä frequency and LADCP profiles show short vertical scales

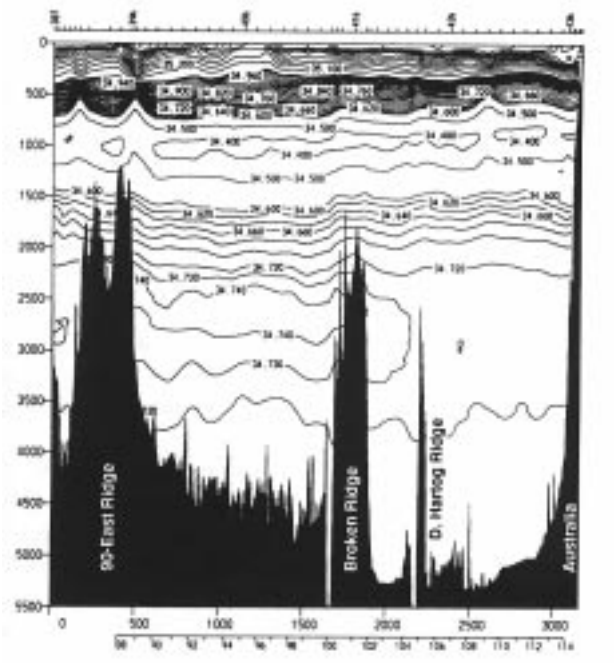

Figure 1b. Salinity along I5E at 32°S.

to the ocean bottom within 3 degrees of the equator like in the Pacific and Atlantic Oceans, suggesting stacked equatorial jets (Luyten and Swallow, 1976). Just south of the equator is a strong eastward equatorial countercurrent, with surface velocities >70 cm s^{-1} based on both ADCP and geostrophic shear. This current extends to about 1100 m; its eastward transport is about 55 Sv, with 18 Sv in the upper 100 m.

A strong front at about 10°S separates the tropical waters from the Indonesian throughflow jet. This jet lies between 10° and 14°S and appears to extend zonally westward from Java, carrying a surface-to-intermediate layer of relatively fresh water. Oxygen and nutrients in the jet are similar to those of the tropical Indian Ocean. On the southern side of the jet is a marked front in oxygen and nutrients, with oxygen increasing towards the south from 2.5 ml/l to 4.5 ml/l at 400 m across 1 degree latitude. The low salinity extends through the Antarctic Intermediate Water (AAIW) level, although the jet's low salinity core is separated from the fresh AAIW core south of 18°S. We identify the core as being of throughflow rather than AAIW origin because of its low oxygen and higher density. Fieux *et al.* (1994) observed properties similar to the jet core near Java and concluded that it was a mixture of low oxygen North Indian Deep Water and Banda Sea Intermediate Water. The throughflow jet has the largest surface dynamic height signature on both sections, with a 50 cm increase and westward surface geostrophic velocities >30 cm s^{-1}; the ADCP suggests 70 cm s^{-1}. Geostrophic transport is 21 Sv westward in the top 1500 m, with 6 Sv in the upper 100 m.

South of 14°S lies the subtropical gyre. A strong oxygen maximum exists to the south along I8N and I5E sections centred at 26.8σ_θ; this is the northward extension of the Subantarctic Mode Water (SAMW) which is ventilated in the southeastern Indian Ocean. A weak O_2 minimum at the same density extends well north of 14°S. This is the densest water which ventilates the subtropical gyre in the Indian Ocean. Along the I5E section the SAMW is also marked by a potential vorticity minimum, reflecting its origin as a deep convective layer north of the Subantarctic Front.

The upper subtropical gyre contains the saline Subtropical Underwater extending equatorward from the subtropical evaporation cell. South of a front at 24°S, the highest salinity is at the surface, and rises to greater than 36.1 psu east of 100°E. Below 100 m along I5E there is almost no variation in water properties on isopycnals down to the AAIW core, which has very slightly lower salinity east of 90°E (Fig. 2).

On the eastern end of the I5E section is the southward-flowing Leeuwin Current. Net transport relative to the bottom is 12 Sv, and is confined to within 2–3 degrees of the coast and to the upper 1200 m. Beneath it the flow is weak (Fig. 3).

The intermediate depths are dominated by AAIW, which extends northward to about 24°S before truncating north of 20°S by the throughflow jet and by the saline Indian Ocean Deep Water extending southward from its origin in the north (Red/Arabian Sea). The global distribution and importance of the tropical boundary near 20°S for AAIW are being described elsewhere.

Sources of deep water for the Central Indian Basin

The Central Indian Basin is far removed from the southern bottom water source since its bottommost water is fed from the east across the Ninety-East Ridge (Warren, 1981, 1982). Warren (1982) showed the importance of a sill at 11°S, compared with a smaller sill at 5°S. Toole and Warren (1993) showed that there could be a small leakage into the Central Indian Basin around 28°S. Our section confirms the importance of the 11°S sill – the largest puddle of water at 80°E with temperature <1°C is centred at 9°S (Talley, 1995), accompanied by the largest deep isopycnal slopes, suggests an 11°S source. A secondary bottom puddle of cold water lies at 18°S; this is probably a southward extension of the 11°S bottom water (Warren, 1982). The mounding of the Central Indian Basin's deep waters in the middle is characteristic of bottom waters in almost all deep basins of the world ocean except in the presence of strong boundary currents or the ACC. The geostrophic shear is cyclonic within the deep basin (anti-

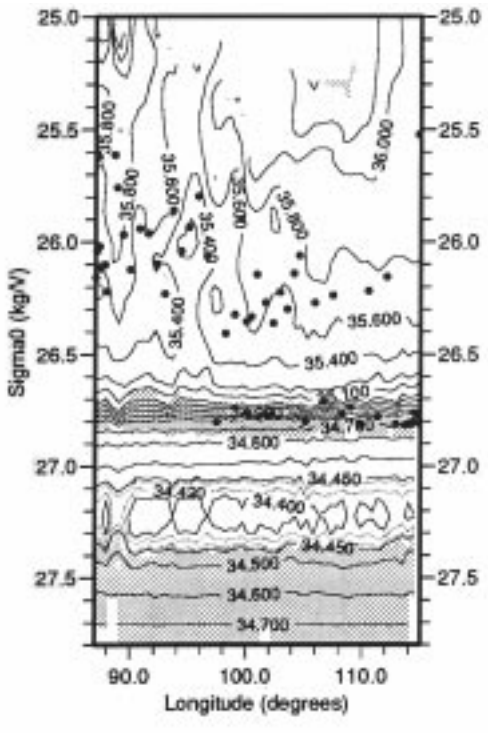

Figure 2. Salinity along the 1995 I5E section with sigma theta as the vertical coordinate. Dots represent the O_2 maximum, marking more recently ventilated waters. Planetary potential vorticity with values less than 60 E-14 (cm s)$^{-1}$ are shaded, also marking waters of convective origin.

cyclonic flow around the ridges) relative to the bottom.

We found clear evidence of westward flow of bottom water through the 28°S sill into the Central Indian Basin, where it turns to the south. A preliminary, heuristic combination of geostrophic shear and LADCP velocities from the three sill sections suggests a bottom flow on the north side of the central section (probably due to a northern location of the deep channel to the east); the deep flow was 3200 to 4000 m deep, 30 km wide, and 10 cm s^{-1}. An origin east of the Ninety-East Ridge and north of Broken Plateau is indicated by the properties; the layer is colder than 1.2°C, fresher than 34.725 psu and denser than 45.89σ_4. The net transport appears to be about 2 to 2.5 Sv.

The deep water lying above the bottom water does not follow such a circuitous route from the south, but rather enters the Central Indian Basin directly across a saddle at about 35°S. The 1987 section (Toole and Warren, 1993) shows its high salinity and high oxygen, centred at 3000–3500 m.

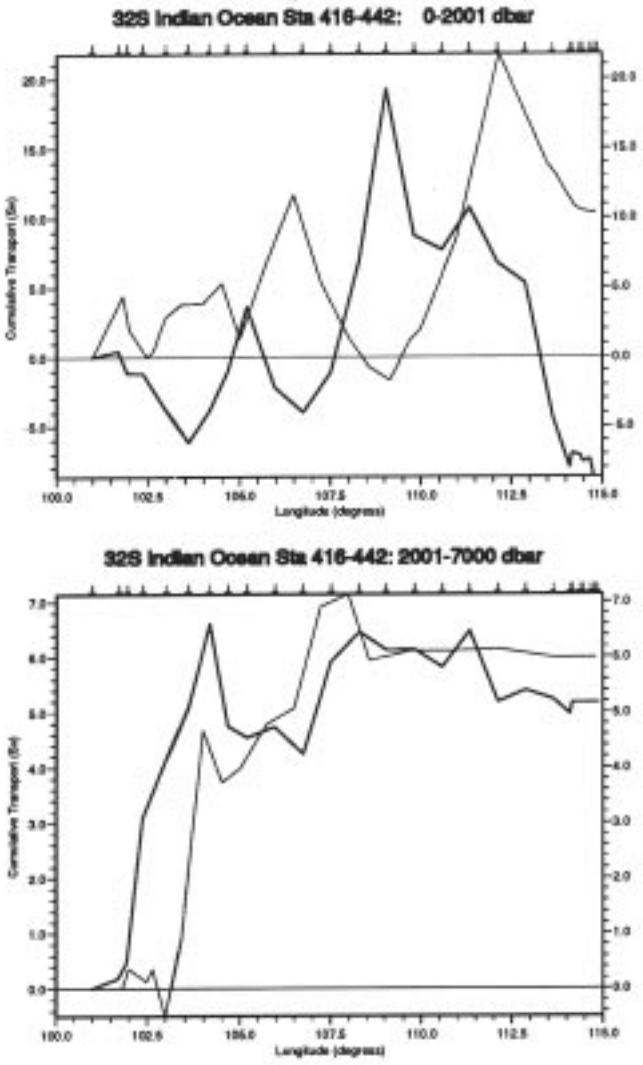

Figure 3. Cumulative geostrophic transport into the Perth Basin (positive values are northward), (a) above 2000 dbar and (b) below 2000 dbar for the 1995 I5E section (heavy) and the 1987 I5 section (light). Reference levels chosen are described in this text and follow Toole and Warren (1993).

Comparison with the 1987 occupation of I5E

The eastward leg of our cruise (Fig. 1b) criss-crossed the 1987 section (Toole and Warren, 1993). The deep flow is northward just east of Broken Ridge on both sections, and southward farther to the east up to Australia, based on property distributions, which show the newest deep and bottom waters banked to the west against Broken Ridge with older waters to the east. Oxygen and nutrients from the new 1995 section show that the northward 2000–4000 dbar flow is confined west of the small Dirck Hartog Ridge. They also show that the deep water which flows north into the Perth Basin is not as new as the deep water which remains south of Broken Plateau.

Preliminary transport calculations follow the spirit of Toole and Warren (1993). Unlike the 1987 section, the deep flow does not narrow significantly with depth. A shallow zero velocity level above the high silica west of the Dirck Hartog Ridge sends this flow northward. Following the break to high silica values the reference is moved deeper to 3000 and 4000 m at Stas 422 and 423. Immediately next to the Ridge a shallower reference near 2500 m reduced the unresolved deep flows to small southward values. To the east of the Ridge deep isopycnals generally slope downward into the Australian coast as was seen in the 1987 section. To produce deep southward flow, a reference level of 4000 m was chosen except near the Australian coast where the deep isopycnals abruptly rise into the coast (also seen in the 1987 section) where a 3000 m reference level was chosen. The net northward flow is 5.2 Sv below 2000 dbar (6.6 Sv northward in the boundary current; 1.4 Sv southward in the interior) (Fig. 3). Toole and Warren (1993) and Warren (1981) both obtained a net northward flow of 6 Sv (7 Sv boundary current; 1 Sv southward return flow). The general location and magnitude of the deep flows are remarkably similar. Note that at about 107°E Toole and Warren show the last of their boundary current flowing north while the 1995 section shows a northward deep flow of a similar 1.5 to 2 Sv, distinctly separated from the boundary current proper.

The most striking difference between the 1987 and 1995 transports lies above 2000 m. Toole and Warren (1993) found a net northward flow of surface waters closing the subtropical circulation (>10 Sv above 2000 m). However the 1995 section shows a net southward flow of surface waters (>8.5 Sv above 2000 m) east of 109°E. The 1987 section showed a net rise of intermediate isopycnals not seen in the 1995 section: the 26.8 and 27.26σ_θ isopycnals rose from 540 to 380 dbar and 1025 to 850 dbar respectively between 100° and 115°E. The 1995 section shows no net rise of these isopycnals (435 and 970 dbar, respectively). This large difference may reflect seasonal variability in the

Leeuwin current transport, which has a maximum southward flow during March-April (Smith *et al*., 1991). We found 5.8 Sv of southward near surface flow above 150 dbar, similar to the 6.2–6.8 Sv found during March–June 1987 by Smith *et al*. (1991), while Toole and Warren (1993) report only 0.7 Sv southward during the opposite season.

Isopycnal salinities in and above the SAMW (26.6–26.8σ_θ) were higher by about 0.05 psu in 1995 compared with 1987. Silica was about 3 umol/kg higher and oxygen was about the same. At greater densities, from the core of the AAIW down to just above the high salinity Circumpolar Water, salinity in 1995 was about 0.01 psu higher than in 1987. Silica was about 5 umol/kg higher and oxygen 0.1 to 0.2 ml/l lower in 1995 compared with 1987. The core of the saline CPW and the waters below to the bottom were fresher by about 0.003 to 0.005 psu. Silica was 5 umol/kg higher, and oxygen was 0.1 ml/l lower in 1995 compared with 1987. If these two sets of measurements are comparable in accuracy, and it is expected that they are, then it appears that from the AAIW down to the bottom, the waters measured in 1995 were older than in 1987.

References

Fieux, M., C. Andre, P. Delecluse, A.G. Ilahude, A. Kartavtseff, F. Mantisi, R. Molcard, and J.C. Swallow, 1994: Measurements within the Pacific-Indian Oceans throughflow region. Deep-Sea Res., 41, 7, 1091–1130.

Fu, L.-L., 1986: Mass, heat and freshwater fluxes in the South Indian Ocean. J. Phys. Oceanogr., 16, 1683–1693.

Knox, R.A., and D.L.T. Anderson, 1985: Recent advances in the study of the low-latitude ocean circulation. Prog. Oceanogr., 14, 259-317.

Luyten, J.R., and J.C. Swallow, 1976: Equatorial undercurrents. Deep-Sea Res., 23, 999–1001.

Smith, R.L., A. Huyer, J.S. Godfrey, and J.A. Church, 1991: The Leeuwin Current off Western Australia, 1986–1987. J. Phys. Oceanogr., 21, 323–345.

Talley, L.D., 1995: WHP sections I8N/I5E in the central Indian Ocean. Internat. WOCE Newsletter, 20, 25–26.

Toole, J.M., and B.A. Warren, 1993: A hydrographic section across the subtropical South Indian Ocean. Deep-Sea Res., 40, 1973-2019.

Warren, B.A., 1981: Deep circulation of the World Ocean. In Evolution of Physical Oceanography, MIT Press, 6–41.

Warren, B.A., 1982: The deep water of the Central Indian Basin. J. Mar. Res., 42 (Suppl)., 823–860.

Warren, B.A., 1994: Driving the meridional overturning in the Indian Ocean. Deep-Sea Research, 41, 9, 1349–1360.

Maurice Ewing Symposium on 'Applications of Trace Substance Measurements to Oceanographic Problems'

Peter Schlosser, Lamont-Doherty Earth Observatory of Columbia University, Palisades, NY 10964-8000, USA

In mid-October 65 scientists from seven countries met at the seventh Maurice Ewing symposium to consider the applications of the measurement of trace substances to oceanography. Anticipating the acquisition of the management of Biosphere 2, Columbia University scientists Schlosser, Smethie and Broecker decided to use this symposium to assess the potential of this site for scientific meetings. The organizers were pleased with the results. Not only were the participants wowed by the host of new results and challenged by syntheses of existing tracer data sets but they were captivated by the beauty of the site, the friendliness of its personnel, and the mystique of the Biosphere itself. The meeting was a great success.

Wally Broecker, a pioneer in this field, was particularly pleased to see that tracer oceanography was at last coming of age. For too long it had remained a prodigal son not fully embraced by the physical oceanographic community. The blossoming of this field awaited the development of numerical models capable of simulating tracer fields. This effort has its roots over a decade ago in work by the modelling groups at Princeton and at Hamburg, but only in the last few years has the interplay between observation and models become a two-way street. Modellers are making use of tracers to verify and improve their simulations, and observationalists are taking note of the power of the models in designing strategies for future tracer measurements. Long convinced that the power of tracer measurements lay primarily in its application to basin and larger scale oceanographic processes, the organizers were pleased to note the greater emphasis being placed on this way of looking at the results.

The meeting topics included global circulation, thermocline ventilation, deep water formation, boundary currents, oceanic variability, integration of tracers in models, tracer release experiments, ocean/atmosphere gas exchange, tracers as proxies for anthropogenic CO_2, and new technologies and methodologies. It was clear that the production of the WOCE data set, which will provide the first 'complete' global tracer survey with high spatial resolution, is well underway. WOCE tracer data are available in the community and are already widely used, especially by a new generation of young scientists who are educated in physical oceanography or ocean modelling. Faster delivery of tracer data to the WOCE data centres was strongly encouraged as a means to efficiently integrate these data into a larger synthesis effort.

Coloured maps of the Helium and Tritium distribution in the Pacific are available on the World Wide Web:
http://kopernik.whoi.edu/wpac/wpac.html

Air-Sea Flux Fields Workshop

Peter K. Taylor, Southampton Oceanography Centre, Empress Dock, Southampton SO14 3ZH

A WCRP sponsored workshop on "Air-Sea Flux Fields for Forcing Ocean Models and Validating GCMS" was held at ECMWF, Reading from 24-27 October. The meeting, organised by Glenn White (NMC) assisted by Peter Taylor (SOC) and Tim Liu (JPL) was timed to directly precede the WGNE meeting, also at ECMWF. The Workshop proceedings will be published in the WCRP Report series.

The stated aims of the workshop were:

(a) To increase interaction between producers and users of surface fluxes

(b) To identify sets of surface flux fields (or fields of the surface meteorological variables) presently available for forcing ocean circulation models on ocean basin to global scales and to determine the advantages and disadvantages of each set.

(c) To devise, through dialogue between flux experts and flux users, a strategy for validating the coupling of ocean and atmosphere models.

(d) To make recommendations for future action and research on air-sea fluxes.

Over 50 participants listened to invited talks grouped under the categories of: the "Surface flux needs of models", the "Assessment of existing estimates of surface flux fields", "Using budgets as a constraint on surface fluxes", the "Accuracy of model derived fluxes", and "How to verify fluxes". The meeting then split into working groups. The main recommendations were:

1. That a limited-life working group on observed air-sea fluxes be set up and that it report to the JSC.
2. The group would catalogue all available data sets related to estimates of global surface fluxes for use in ocean and coupled models. The group would generate a summary of data set availability and accuracies, indicate the strengths and weaknesses of the data sets and identify the accessibility and cost of the data sets.
3. The group would conduct, in cooperation with other groups, an intercomparison and evaluation of all available flux estimates for the period 1979 to the present. A main component of this intercomparison would be the evaluation and comparisons with other flux estimates of air-sea fluxes from the reanalyses by atmospheric data assimilation systems.
4. The group would conduct an intercomparison of fluxes from different point bulk formulae parameterizations and from different model bulk formulae parameterizations, using a few selected data sets.
5. The group would report to a future air-sea flux workshop.

Meeting Timetable 1996

WOCE Meetings

February 5-9	DPC-9	Brest
April	SMWG-2	Grenoble
April 15-17	US SSC	Washington, DC
April 15-19	UOT-DAC-6/GTSPP-4	Washington, DC
May 14-17	SVP-8	Toulouse
August 19-23	WOCE Pacific Workshop	Newport Beach, CA
October 7-9	WHP-15	Woods Hole, MA
October 15-17	WOCE-23	Southampton, UK

Science and other Meetings

January 22-26	International Symposium on CO_2 in the Oceans, Puerto Rico
February 12-16	Ocean Science Meeting, San Diego
March 5-8	Oceanology International '96, Brighton
March 11-16	WCRP JSC-XVII, Toulouse
May 6-10	XXI Assembly of the European Geophysical Society, Den Haag
July 8-11	TOS Meeting on Marine Environment and Global Change Programmes, Amsterdam
July 23-27	AGU Western Pacific Geophysics Meeting, Brisbane
August 13-16	Pacific Ocean Remote Sensing Conference, Victoria, CA

For more information on the above meetings contact the IPO. If you are aware of any conferences or workshops which are suitable for the presentation of WOCE results and are not mentioned in the above list please let the IPO know.

Note on Copyright

WOCE is a component of the World Climate Research Programme (WCRP), which was established by WMO and ICSU, and is carried out in association with IOC and SCOR. The scientific planning and development of WOCE is under the guidance of the JSC Scientific Steering Group for WOCE, assisted by the WOCE International Project Office. JSC is the main body of WMO-ICSU-IOC, formulating overall WCRP scientific concepts.

The WOCE Newsletter is edited at the WOCE IPO at the Southampton Oceanography Centre, Empress Dock, Southampton SO14 3ZH (Tel: 44-1703-596789, Fax: 44-1703-596204, e-mail: woceipo@soc.soton.ac.uk).

We hope that colleagues will see this Newsletter as a means of reporting work in progress related to the Goals of WOCE as described in the Scientific Plan. The SSG will use it also to report progress of working groups, experiment design and models.

The editor will be pleased to send copies of the Newsletter to institutes and research scientists with an interest in WOCE or related research.